Supporting Information

Nanoceria-Based Phospholipase-Mimetic Cell Membrane Disruptive Anti-Biofilm Agents

Kritika Khulbe[‡a], *Kapudeep Karmakar*[‡†bc], *Sourav Ghosh*[a], *Kasturi Chandra*[b], *Dipshikha Chakravortty**[bd] *and Govindasamy Mugesh**[a]

[a] Department of Inorganic and Physical Chemistry, Indian Institute of Science, Bangalore 560012, India

[b] Department of Microbiology and Cell Biology, Indian Institute of Science, Bangalore 560012, India

[c] Regional Research Station, Terai Zone, Uttar Banga Krishi Viswavidyalaya-ICAR, Coochbehar 736165, West Bengal, India

[d] Center for Biosystem Science and Engineering Indian Institute of Science, Bangalore 560012, India

† Present Address: Uttar Banga Krishi Viswavidyalaya, Pundibari, Coochbehar, West Bengal 736165

‡These authors contributed equally.

*Corresponding authors:

dipa@iisc.ac.in, mugesh@iisc.ac.in

Table of Contents

1. Chemicals

Cerium chloride heptahydrate ($CeCl_3.7H_2O$) was purchased from Avra synthesis Pvt. Ltd. Cerric ammonium nitrate ($(NH_4)_2Ce(NO_3)_6$), ethylenediamine, hydrazine hydrate and ammonium hydroxide, 3-aminopropyltriethoxysilane used for various synthesis were purchased from Sisco Research Laboratories. Sodium polyacrylate and flouresceine isothiocynate used for preparing PAA-Cnp and FITC-tagged PAA-Cnp nanoparticles respectively were purchased from Sigma Aldrich. Trizma base and phosphotidyl choline (lecithin) used for hydrolysis assays were also purchased from Sigma Aldrich. 1-Palmitoyl-2-oleoyl-sn-glycero-3-phosphoglycerol and p-nitrophenyl phosphorylcholine used for other hydrolysis assays were purchased from TCI Co. Ltd. and Alfa Aesar Fischer Scientific respectively.

2. Characterization Methods

Scanning electron microscopy (SEM) and EDX spectrawere performed on a Carl-Zeiss Ultra 55, FEI Sirion UHR SEM and ESEM-Quanta instruments,respectively. Transmission electron microscopy (TEM), high resolution TEM (HRTEM), electron diffraction X-Ray (EDX) analysis and selected area electron diffraction (SAED) were recorded on JEOL transmission electron microscope operating at 200 kV after casting a drop of nanoparticle dispersion in acetone over Cu grid. Powder XRDwas recordedon Philips PANalytical X-ray diffractometer by using a Cu-Kα (1.5406 Å)radiation. X-ray photoelectron spectroscopy (XPS) was acquired on AXIS ULTRA, KRATOS ANALYTICAL, SHIMADAZU. Raman spectroscopy was performed on HORIBA JOBIN YVON LabRAM HR Raman spectrometer (532 nm laser. FT-IR spectra were recorded on aPerkinElmer FT-IR spectrometer. Zeta potential was measured usingMalvern Zetasizer Nano UK.UV-Vis absorption spectra were acquired onSHIMADAZU UV-2600 spectrophotometer. Fluorescence spectroscopy was measured by using HORIBA JOBIN YVON (Fluoromax-4 Spectrofluorometer) instrument. All the ^{31}P NMR spectra were recorded using AV400 and AV500 MHz Avance Bruker High Resolution Multinuclear FT-NMR spectrometer. Softwares used for data analysis and plotting were CASA XPS, OriginPro 8, ChemDraw Professional 15.1, Chemcraft, TopSpin 3.5pl6 and MestReNova.

3. Electron microscopy of bacterial biofilm

The above procedure was used for the formation of biofilm with a modification that a sterile glass slide (1cm x 1cm) was placed in 12 well in a slanting position resting on wall. The samples were fixed in 2.5% glutaraldehyde at 4ºC for 24 hours. After washing with PBS for three times, the samples were dehydrated in a gradient series of alcohol concentration (30, 50, 60, 70, 80, 90, 95 and 100%) for 15 min at each concentration. The samples were sputter-coated with gold (JEOL JFC-1100E ion sputtering device; JEOL, Tokyo, Japan) and analyzed by scanning electron microscope and analyzed by field emission-SEM (FEI Quanta 200, Eindhoven, Netherlands).

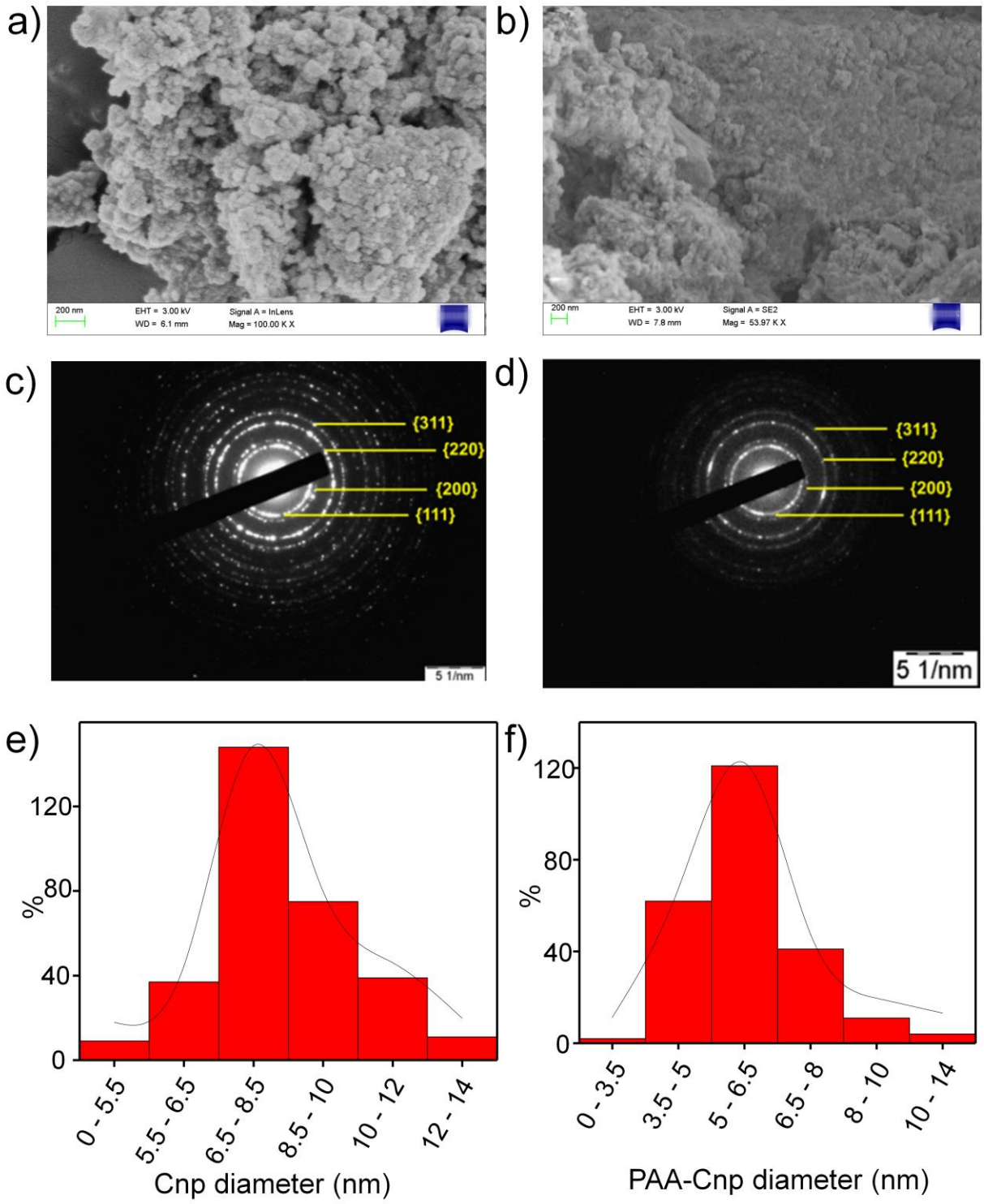

Figure S1: Scanning electron microscopy (SEM) images of agglomerated nanoparticles a) Cnp and b) PAA-Cnp. TEM images and SAED patterns (inset) of sonicated c) Cnp and d) PAA-Cnp. Particle size distribution profile of e) Cnp and f) PAA-Cnp.

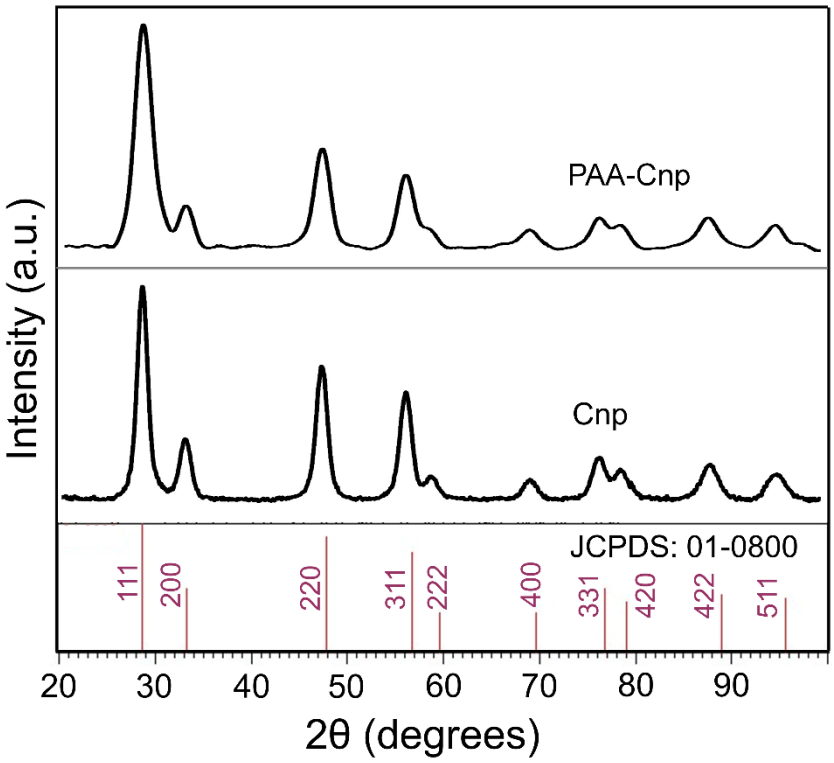

Figure S2: Powder XRD pattern of Cnp and PAA-Cnp indicating cubic flourite lattice (JCPDS No. 01-0800).

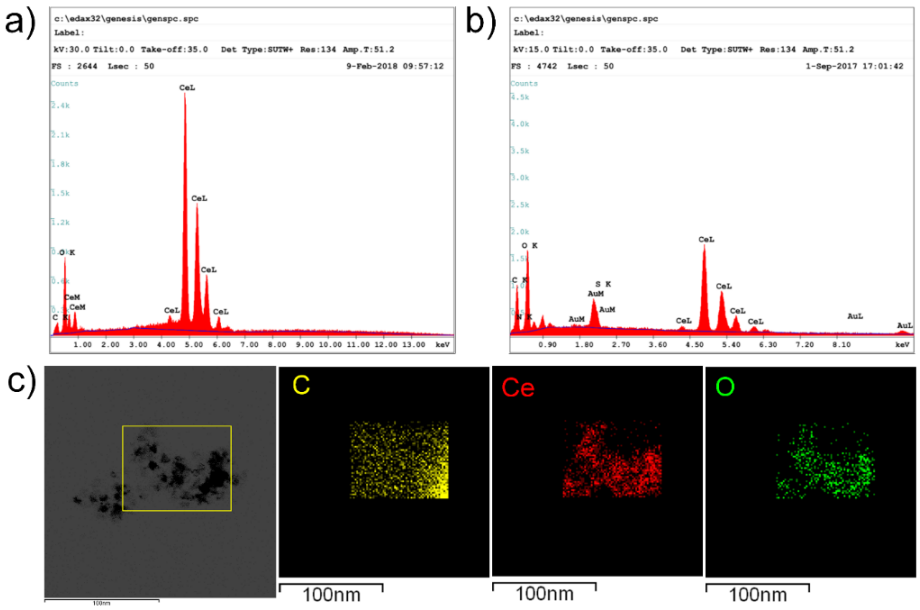

Figure S3: Elemental characterisation by energy dispersive X-ray analysis (EDAX) of a) Cnp and b) PAA-Cnp. c) X-ray mapping shows the distribution of elements Ce, C and O present in PAA-Cnp nanoparticles.

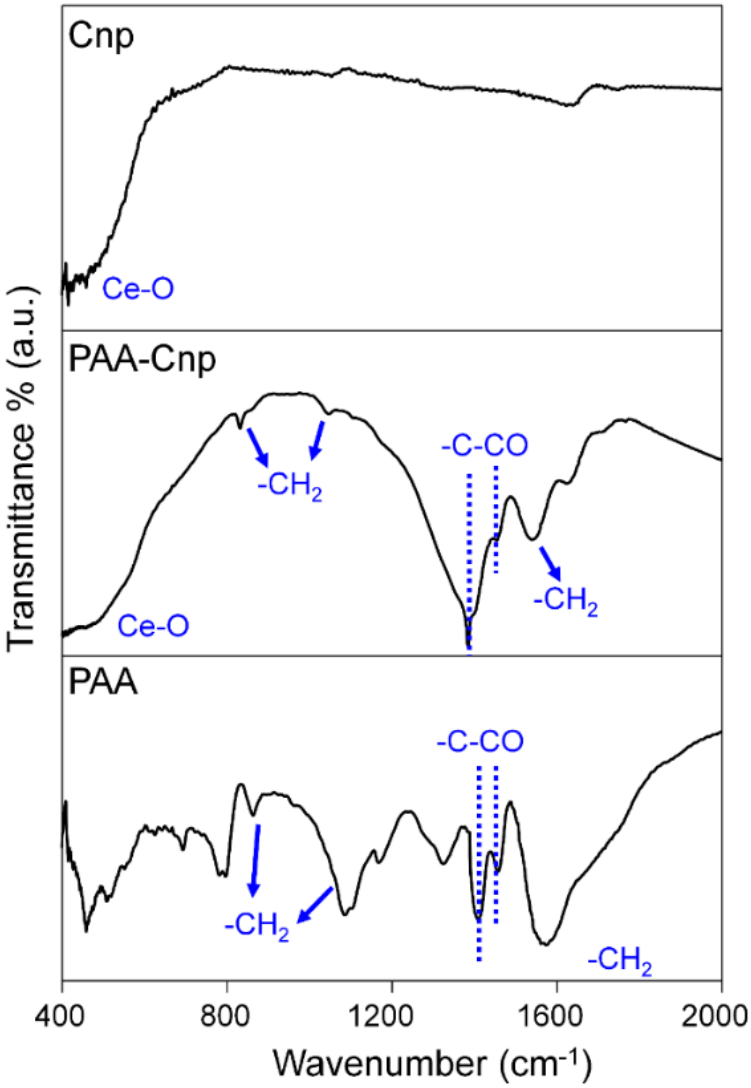

Figure S4: FT-IR spectra of Cnp, PAA-Cnp and PAA. Characteristic peak for Ce-O stretching vibration was observed at 460 cm^{-1} for both Cnp and PAA-Cnp. However, additional peaks were observed in case of PAA-Cnp at 834 cm^{-1}, 1049 cm^{-1}, 1536 cm^{-1} correspond to $-CH_2$ stretching vibrations and at 1382 cm^{-1} correspond to $-C-CO_2H$ stretching vibrations. These peaks matched with the respective peaks observed in case of PAA which confirms the coating of PAA on nanoceria. The presence of $-CO_2H$ stretching in FT-IR spectra of PAA-Cnp can arise due to the mechanical rupturing of PAA attached to Cnp while preparation of KBr pellet of PAA-Cnp (which was not observed in the Raman spectra).

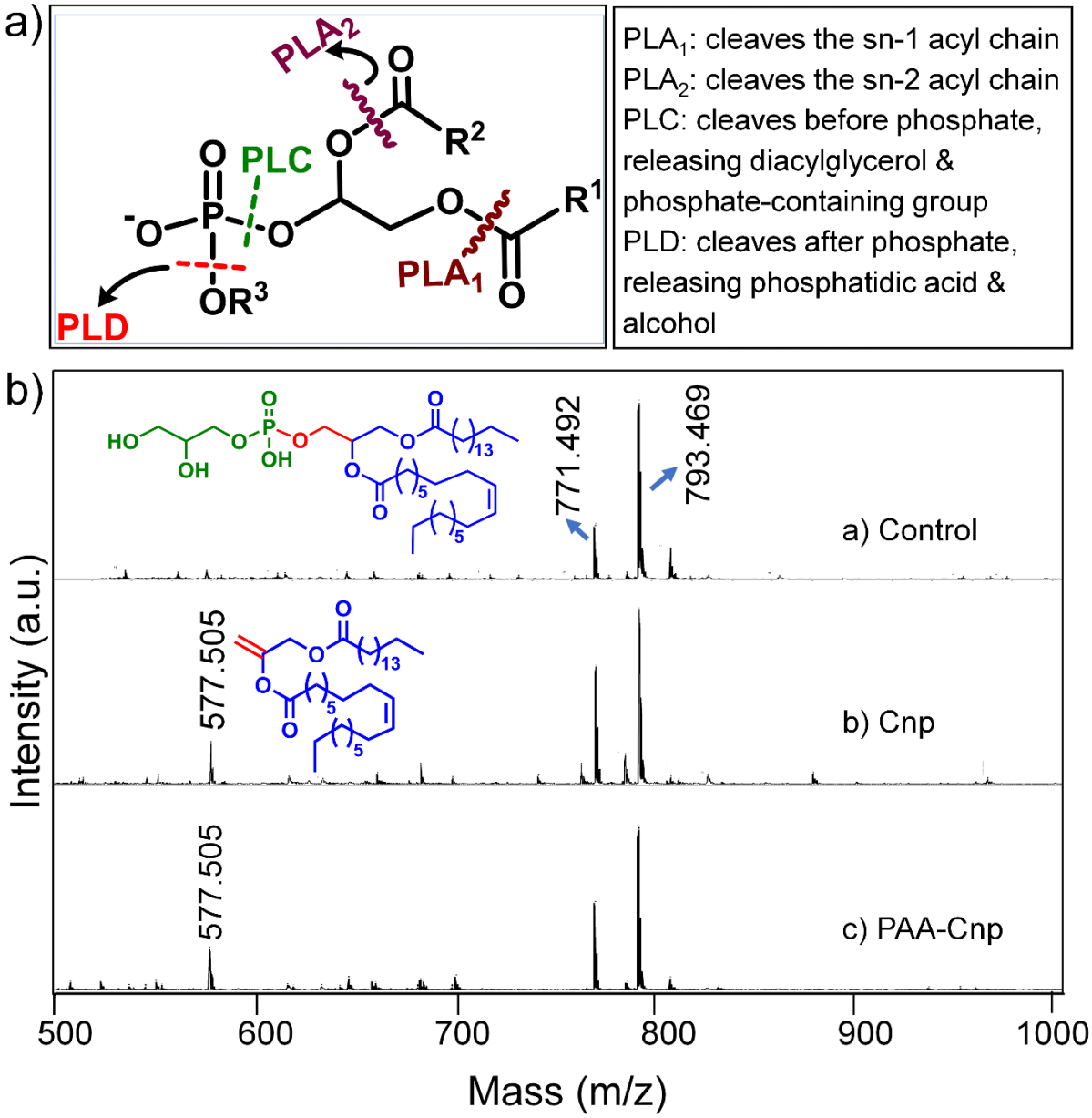

Figure S5: a) Types of phospholipase activities. b) MALDI-Mass obtained after the hydrolysis of 1-palmitoyl-2-oleoyl-sn-glycero-3-phosphoglycerol (POPG) treated with nanozyme, Cnp or PAA-Cnp, in Tris buffer pH 7.8 at 37 °C for 24 h. Unlike control MALDI spectra where peak around 771.5 and 793.5 m/z was obtained for POPG ($M+Na^+$) and ($M+2Na^+$) respectively, additional peak was observed at 577 m/z assigned for 3-(palmitoyloxy)prop-1-en-2-yl oleate ($M+H^+$) formed from the hydrolysis of POPG by the nanozymes via PLC mediated pathway.

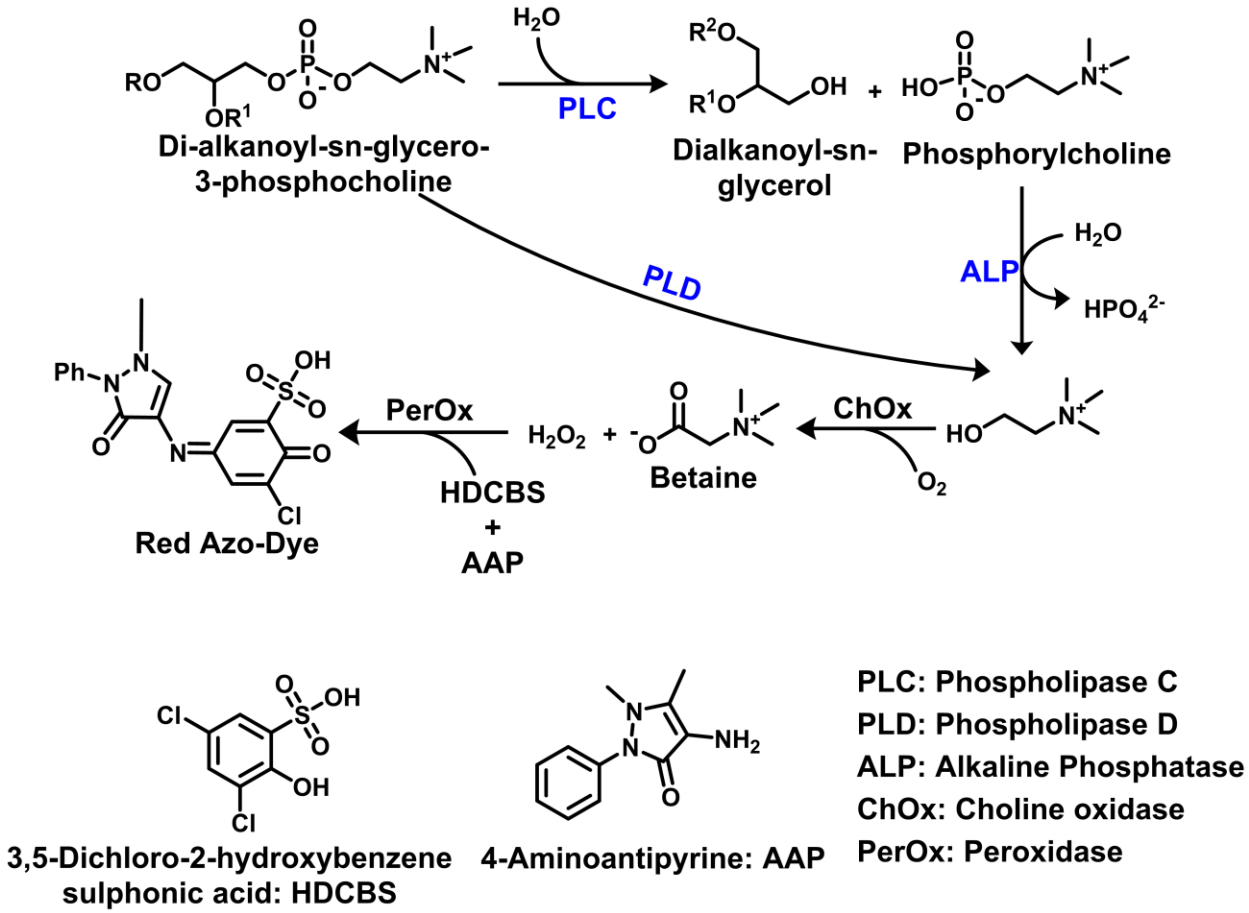

Figure S6: Mechanism of a UV-Vis assay representing of phospholipase C (PLC) and phospholipase D (PLD) activity of enzyme using phosphatidyl choline as substrate. The phosphocholine diester upon hydrolysis by a PLC-mediated pathway gives phosphoryl choline as product whereas *via* PLD-mediated pathway, choline is the hydrolysis product. Unlike PLD, alkaline phosphatase (ALP) enzyme is involved with PLC in the reaction scheme to form choline from phosphatidyl choline. A sequence of enzymatic reactions is involved starting with oxidation of choline by choline oxidase to give betaine and H_2O_2. This H_2O_2 is utilized by peroxidase enzyme to generate hydroxyl radicals which facilitate the radical-mediated azo-dye formation between 2-hydroxy-3,5-dichlorobenzene sulphonic acid sodium salt (HDCBS) and 4-aminoantipyrene (AAP). In both the cases the final product is the formation of red chromogen azo-dye which has characteristic λ_{max} at 508 nm in the absorption spectrum. As, choline oxidase specifically takes choline as a substrate in its active site pocket, therefore, based on whether the product formed in the supernatant solution is choline (by PLD mediated hydrolytic pathway) or phosphoryl choline (by PLC mediated hydrolytic pathway), the dye formation will be observed in the absence or presence of alkaline phosphatase enzyme.

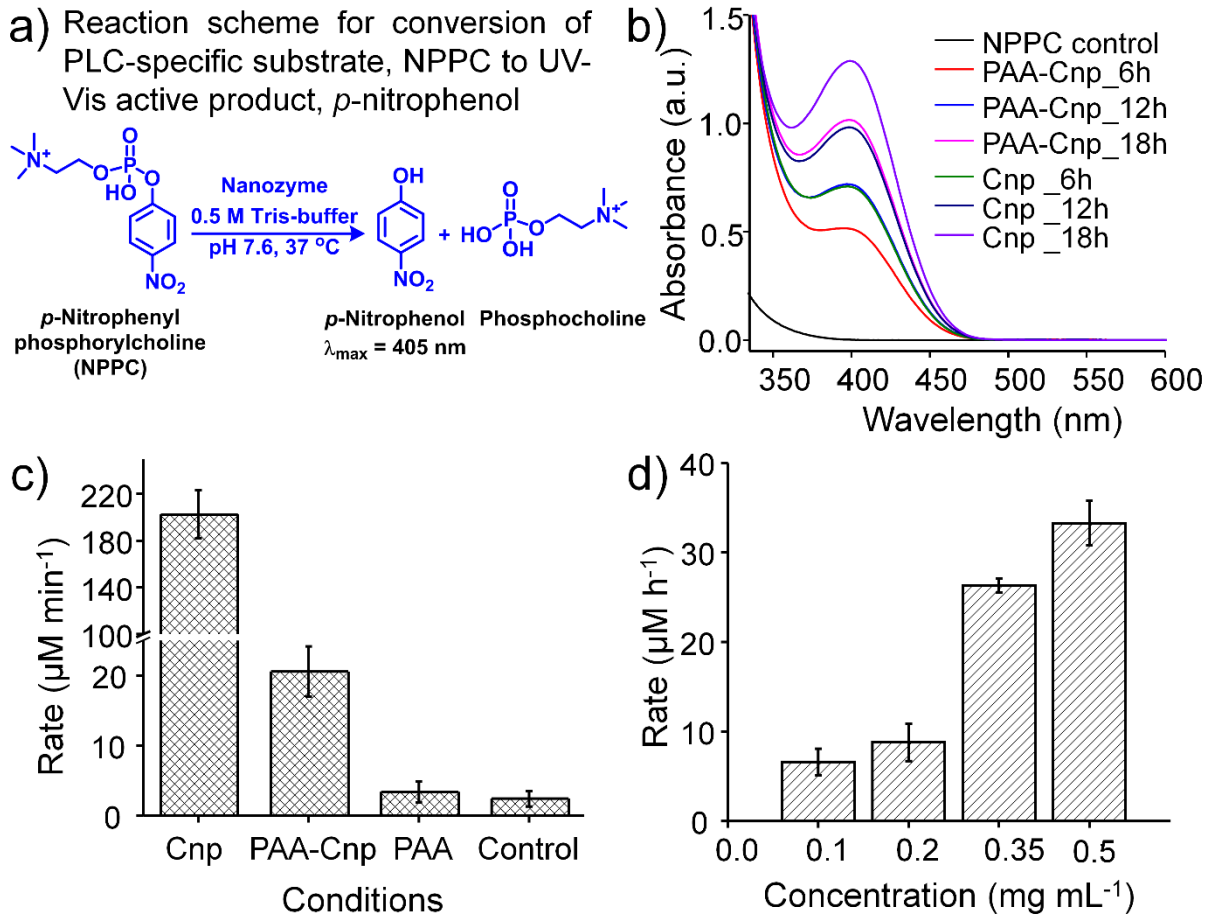

Figure S7: a) Reaction scheme of *p*-nitrophenyl phosphorylcholine (NPPC) hydrolysis by PLC-mimetic nanozymes, Cnp and PAA-Cnp. b) UV-Vis spectra showing absorbance maxima at 405 nm of *p*-nitrophenol formed by hydrolysis of NPPC using Cnp and PAA-Cnp at different time-points, i.e., 6h, 12h and 18h. c) Comparison of initial rate of NPPC hydrolysis in the presence and absence of nanocatalysts, Cnp and PAA-Cnp in the presence of Tris buffer pH 7.8 at 37 °C by monitoring increase in absorbance intensity of peak at 405 nm. d) Bar diagram shows the rate of formation of *p*-nitrophenol from the hydrolysis of NPPC (4.0 mM) by varying concentration of PAA-Cnp in Tris buffer pH 7.8 at 37 °C monitored by UV-Vis spectroscopy at 405 nm. The rate of hydrolysis increases proportionally with the increasing concentration of the nanozyme.

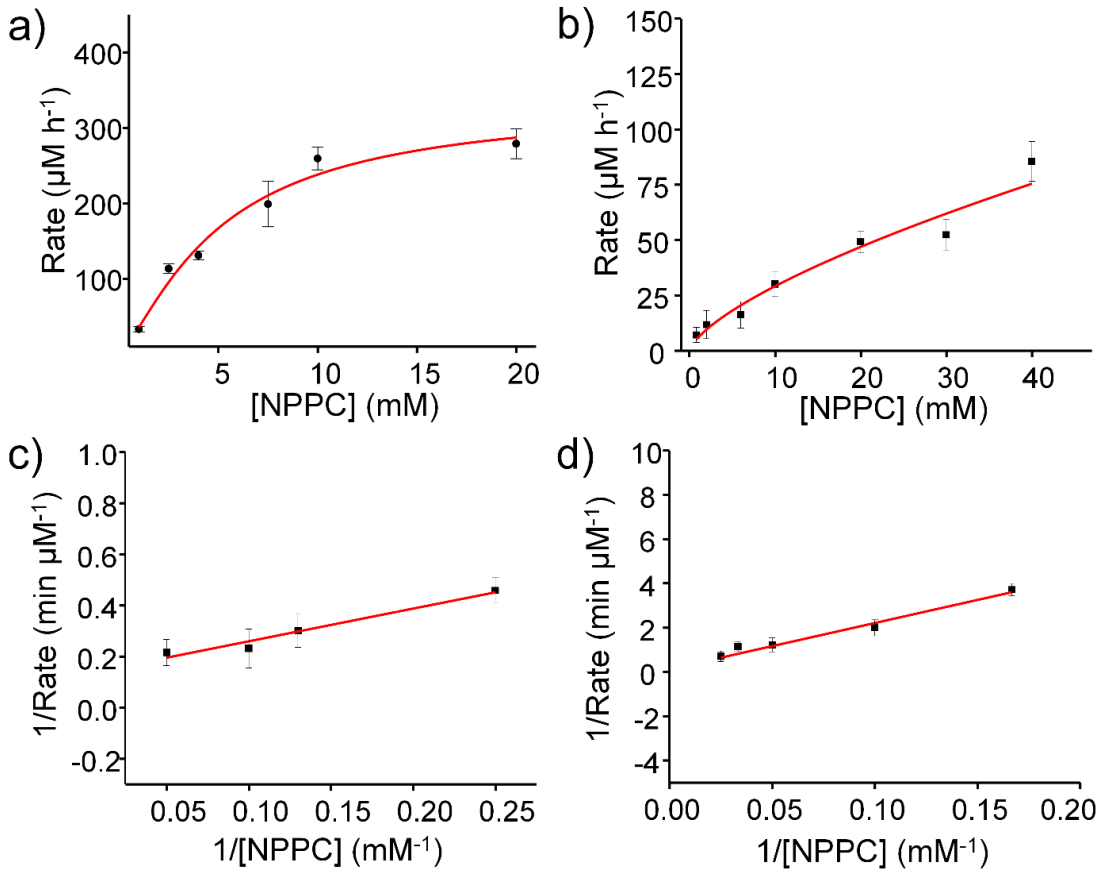

Figure S8: a-b) Michaelis-Menten kinetics observed for Cnp and PAA-Cnp respectively for the hydrolysis of NPPC in Tris buffer pH 7.8 at 37 °C. The rate of NPPC hydrolysis was monitored by measuring absorbance of *p*-nitrophenol formation at 405 nm using UV-Vis spectroscopy. c-d) Lineweaver-Burk plot for Cnp and PAA-Cnp respectively.

Table S1: Catalytic parameters obtained for the hydrolysis of different concentrations of *p*-nitrophenyl phosphoryl choline (NPPC) by PAA-Cnp in Tris buffer pH 7.8 at 37 °C by monitoring the formation of *p*-nitrophenol at 405 nm using UV-Vis spectroscopy.

S.No.	Catalytic Parameter	PAA-Cnp	Cnp
1	K_M (mM)	171.8 ± 1.89	9.8 ± 0.25
2	V_{max} (μM h^{-1})	492 ± 68.4	456 ± 84

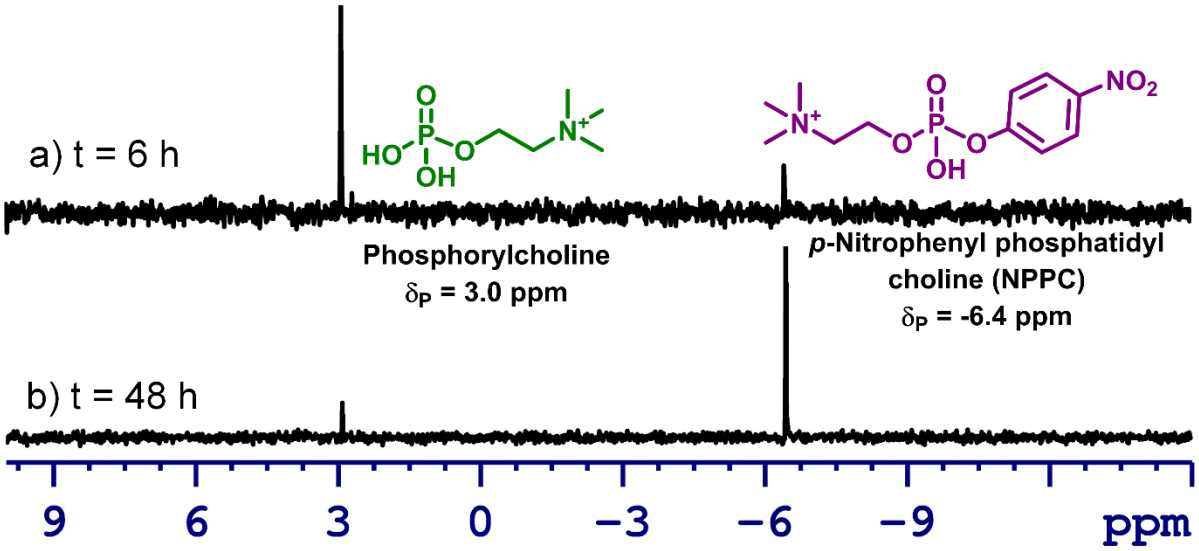

Figure S9: ^{31}P NMR spectroscopy analysis for the hydrolysis of NPPC (1.0 mM) by PAA-Cnp showing formation of phosphoryl choline in Tris buffer pH 7.8 at 37 °C at different time points: a) time= 6 h and b) time= 48 h.

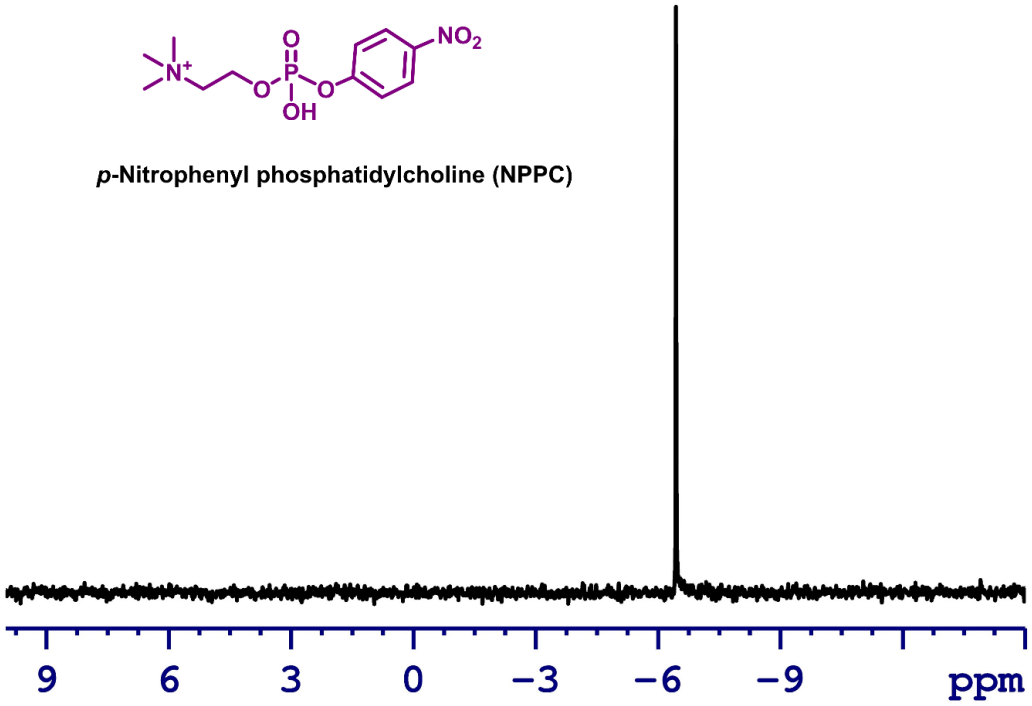

Figure S10: ^{31}P NMR spectra of NPPC (1.0 mM) showing no hydrolysis of substrate to form phosphoryl choline even after 48 h in Tris buffer pH 7.8 at 37 °C.

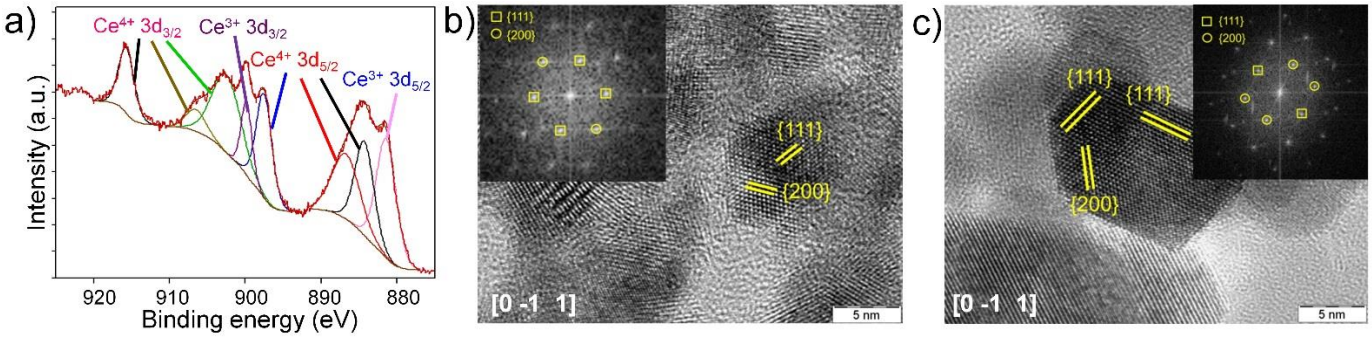

Figure S11: a) X -ray photoelectron spectroscopic analysis of deconvoluted spectra of Ce 3d for PAA-Cnp depicting presence of Ce in both +3 and +4 oxidation states. b) HRTEM and FFT (inset) analysis show {1 1 0} as majorly exposed planes on the surface of PAA-Cnp. c) HRTEM and FFT (inset) analysis show {1 1 0} as majorly exposed planes on the surface of Cnp.

Table S2: Assignment of peaks for Ce 3d deconvoluted XPS spectra of PAA-Cnp nanoparticles.

Binding Energy (eV)	881.4	884.2	886.7	897.5	899.8	902.5	906.5	915.6
Core level value	$3d_{5/2}$	$3d_{5/2}$	$3d_{5/2}$	$3d_{5/2}$	$3d_{3/2}$	$3d_{3/2}$	$3d_{3/2}$	$3d_{3/2}$
Oxidation State	Ce^{3+}	Ce^{4+}	Ce^{4+}	Ce^{4+}	Ce^{3+}	Ce^{4+}	Ce^{4+}	Ce^{4+}

Table S3: Assignment of peaks for Ce 3d deconvoluted XPS spectra of Cnp nanoparticles.

Binding Energy (eV)	881.5	882.9	888.1	897.5	900.0	901.5	907.0	915.9	916.4
Core level value	$3d_{5/2}$	$3d_{5/2}$	$3d_{5/2}$	$3d_{5/2}$	$3d_{3/2}$	$3d_{3/2}$	$3d_{3/2}$	$3d_{3/2}$	$3d_{3/2}$
Oxidation State	Ce^{3+}	Ce^{4+}	Ce^{4+}	Ce^{4+}	Ce^{3+}	Ce^{4+}	Ce^{4+}	Ce^{4+}	Ce^{4+}

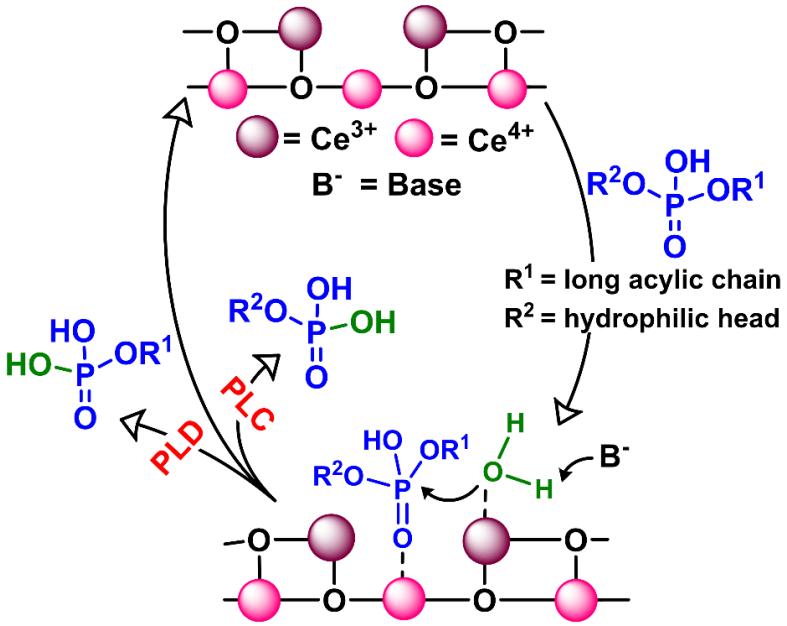

Scheme S1: Schematic representation of the hydrolysis of phosphatidyl choline substrate by PLC and PLD activity on the surface of nanoceria.

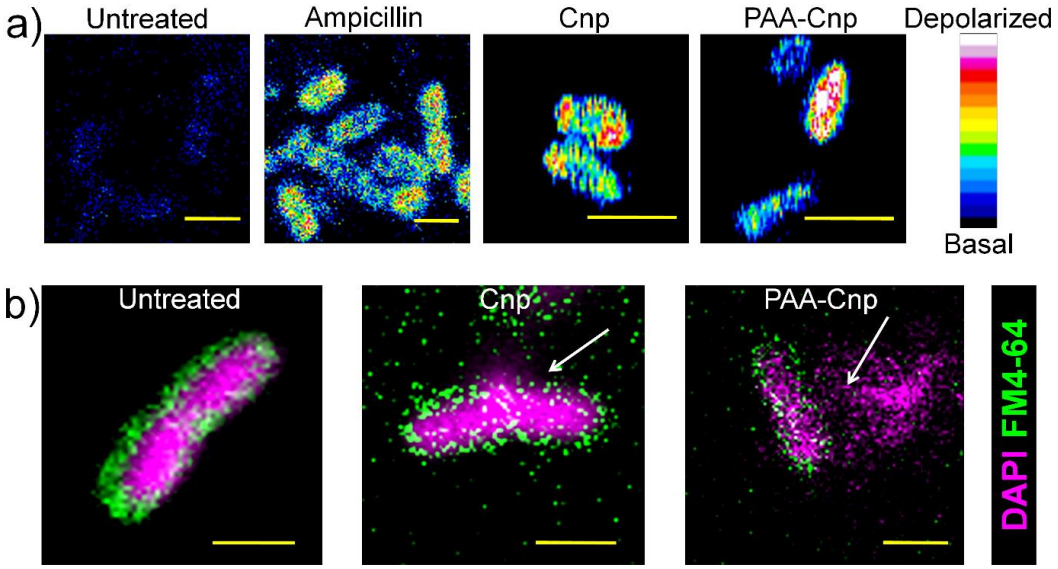

Figure S12: a) Confocal images show depolarization of bacterial cell membrane after treatment with PAA-Cnp using $DiBAC_4$ (3) staining. Ampicillin treated cells were used as a positive control for depolarization in comparison with untreated cells. Scale bar = 2 µm. b) Confocal microscopy images of damaged bacterial cell membrane of *Salmonella* bacteria grown in M9 media respectively, by Cnp and PAA-Cnp. Membrane damage was visualized using FM4-64 dye (for staining lipid bilayer) and DNA leaking from cells was visualized by DAPI.

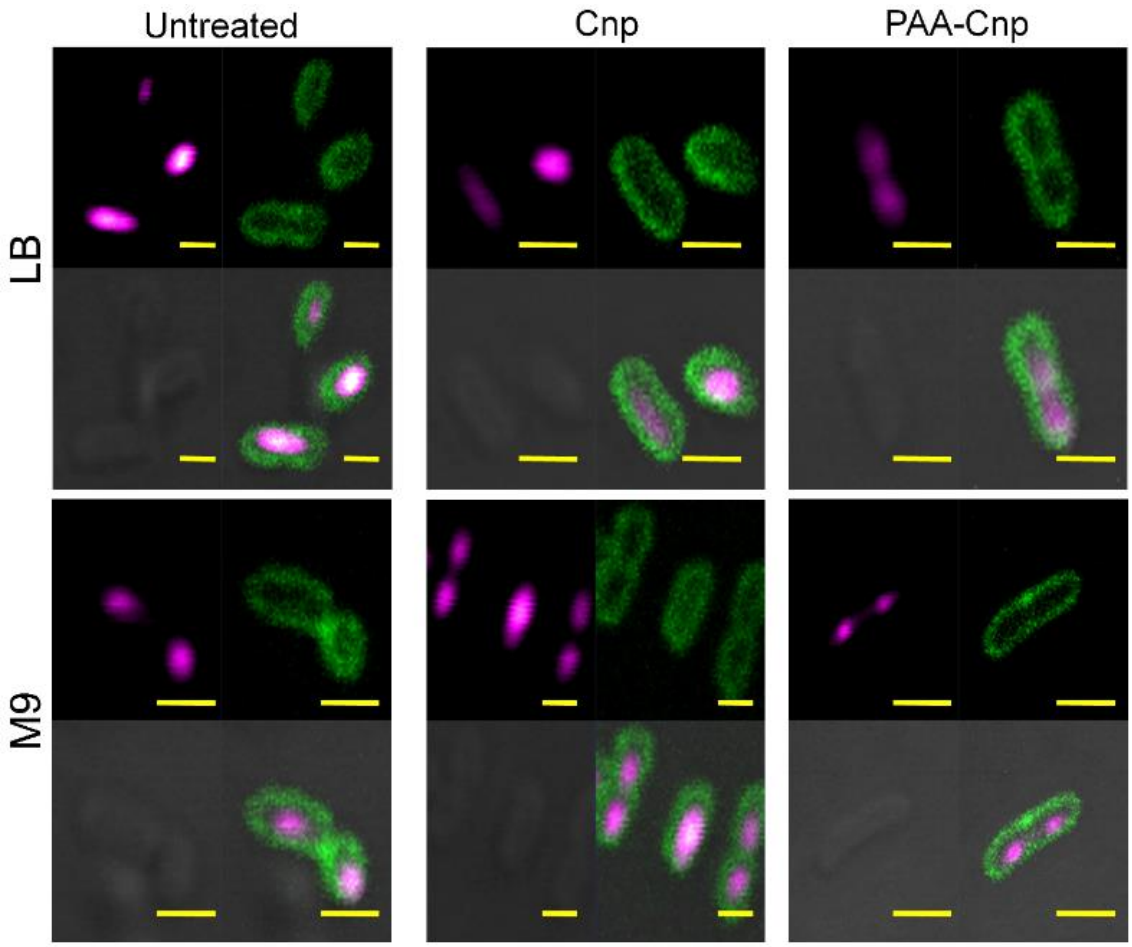

Figure S13: Confocal microscopy images of bacterial cell membrane of *Salmonella* grown till log phase in LB and M9 media pre-treated with Cnp and PAA-Cnp. Membrane was visualized using N-(3-triethylammoniumpropyl)-4-(6-(4-(diethylamino)phenyl) hexatrienyl) pyridinium dibromide (FM4-64) dye (for staining lipid bilayer) and cellular DNA using DAPI (Bottom right panel). No membrane damage was observed in the log-phase which is represented by DAPI encircled within the boundary marked by FM4-64. The pseudo-colours for DAPI (magenta) (top right panel) and FM4-64 (green) (top left panel) have been used in the image to obtain proper contrast between different cellular regions. DIC images of the bacteria are shown in the bottom left panel. Scale bar = 1µm.

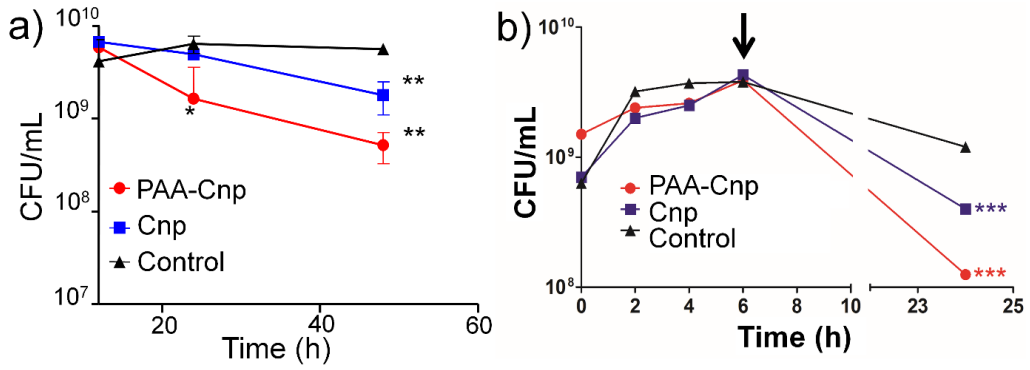

Figure S14: a) CFU analysis of Salmonella in the stationary phase grown in LB media upon treatment with 50 µg/mL of Cnp or PAA-Cnp. One-way ANOVA was used to analyze the result. P<0.001=***; P<0.01=**. b) Growth curve of *Salmonella* in M9 media when treated at the stationary phase with 50 µg/mL of Cnp and PAA-Cnp. Arrow indicate the time point when the nanoparticle, Cnp or PAA-Cnp, was added. One way ANOVA with Bonferroni post test was used to analyse the results. P<0.001=***. In both the cases, the nanozymes showed antibacterial activity compared to control. However, the greater reduction in CFU was displayed by PAA-Cnp indicating its enhanced antibacterial activity.

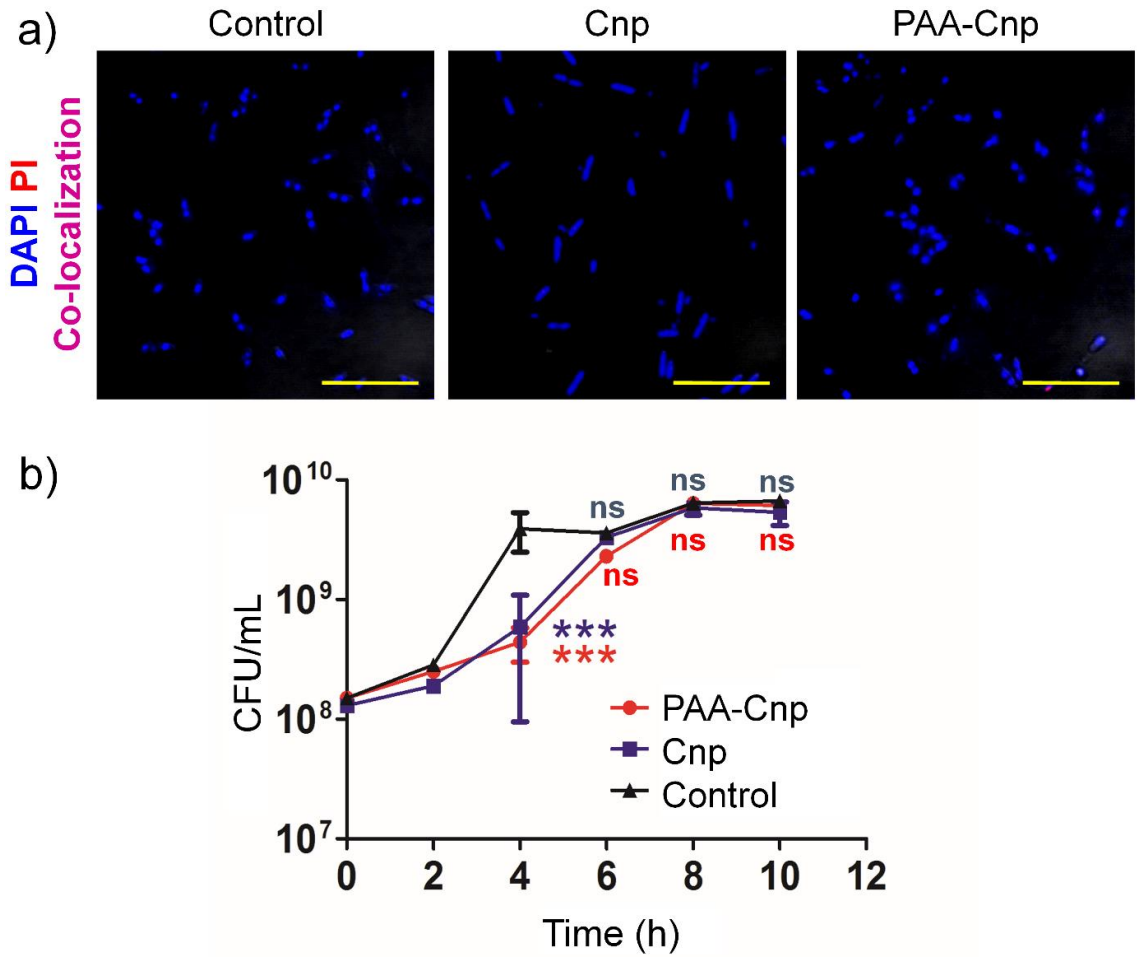

Figure S15: a) Representative confocal image from the log-phase (0.3 $OD_{600\ nm}$) of *Salmonella* stained with 4',6-Diamidino-2-phenylindole (DAPI) and Propidium iodide (PI). DAPI was used to visualize bacteria and PI was used to stain the dead bacterial cells. Very few dead cells was observed in the confocal images indicating no antibacterial activity of the nanoparticles in the log phase which correlates-well with the earlier observation in FigureS10-12. Scale bar=5 µm. b) Growth curve of *Salmonella* in LB when treated with 50 µg/mL of Cnp and PAA-Cnp. A reduction in CFU was observed at 4 h, which was subsequently recovered at later time-points indicating that nanoparticles do not have antibacterial effect on the early growth phase of bacteria. One way ANOVA with Bonferroni post test was used to analyse the results. P<0.001=*** and P>0.05=ns.

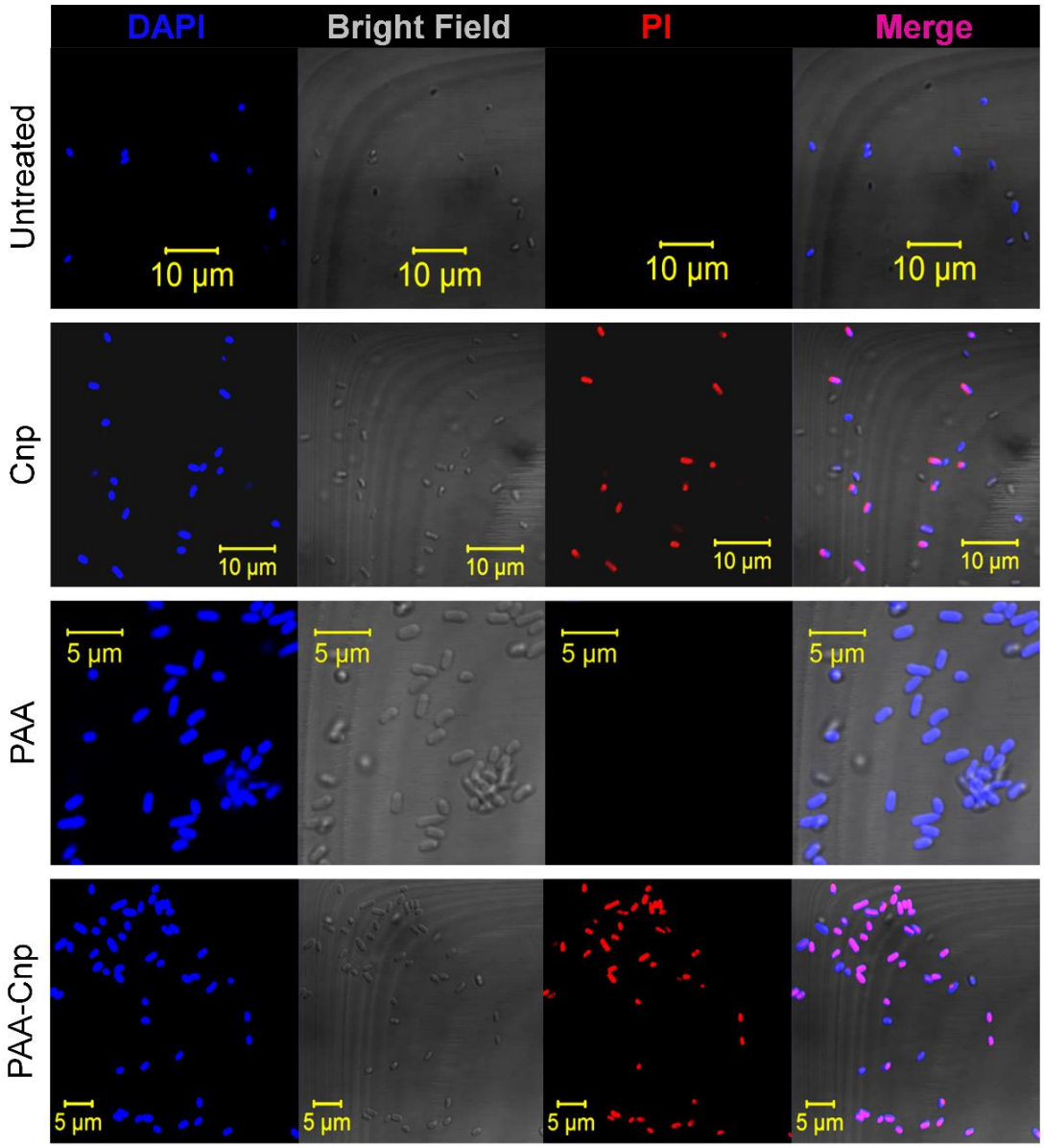

Figure S16: Representative confocal images of *Salmonella* from the stationary phase upon pre-treatment with either PAA, Cnp or PAA-Cnp. DAPI was used to visualize bacteria and PI was used to stain the dead bacterial cells. Antibacterial activity was observed for both PAA-Cnp and Cnp, whereas no cell death was seen in case of control and PAA alone. These results indicate that PAA alone does not contribute to the antibacterial activity of PAA-Cnp.

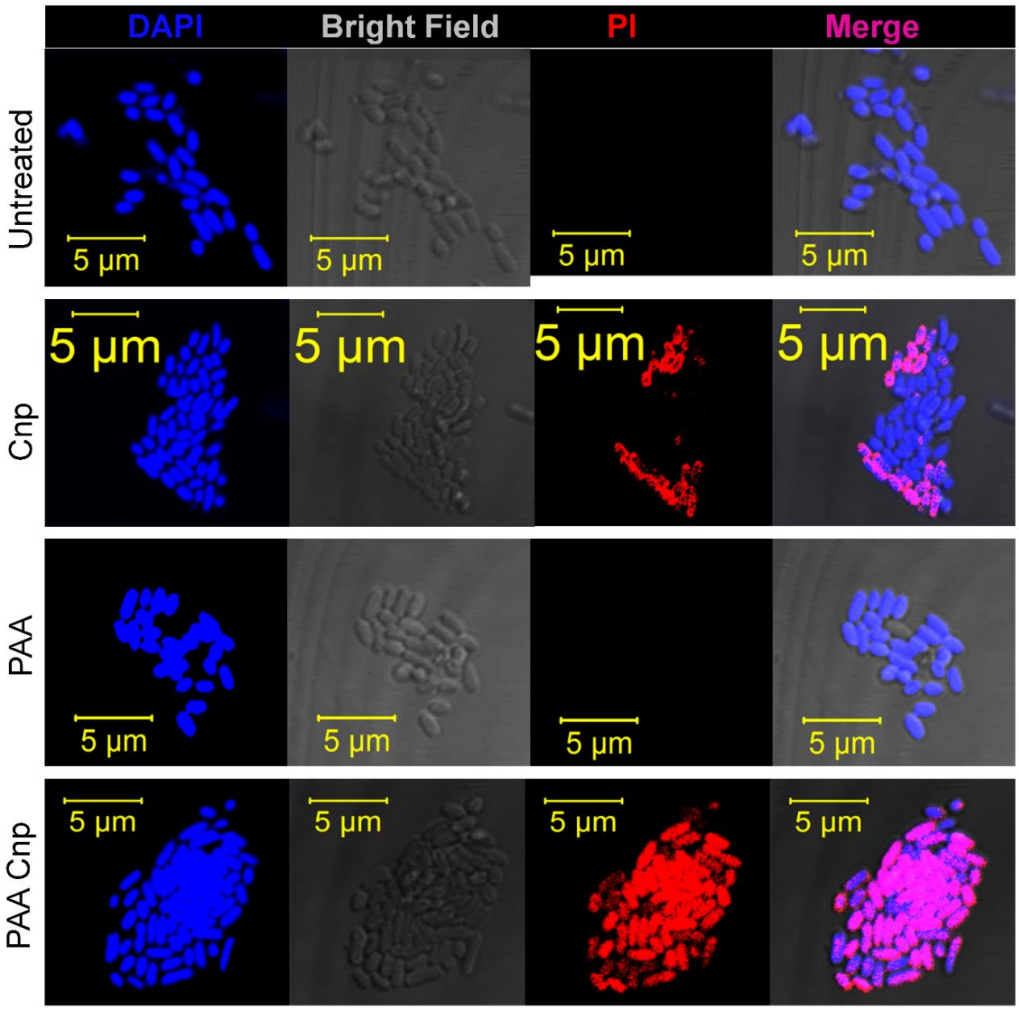

Figure S17: Antibacterial property was observed during initial attachment stage: Representative confocal images of *Salmonella* grown till the stationary phase, attached to cover slip and subsequently treated with either PAA, Cnp or PAA-Cnp. DAPI was used to visualize bacteria and PI was used to stain the dead bacterial cells. Antibacterial activity was observed for both PAA-Cnp and Cnp, whereas no cell death was seen in case of control and PAA alone, at the cellular attachment stage. Also, PAA alone does not contribute to the antibacterial activity of PAA-Cnp.

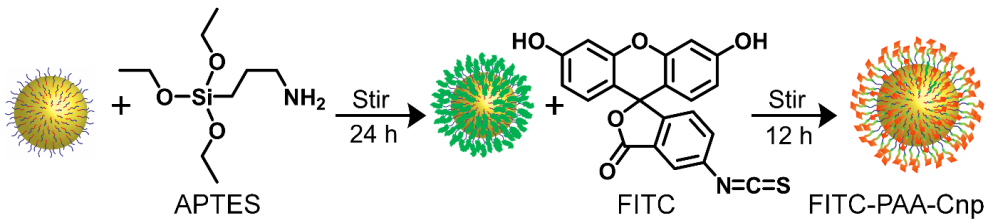

Figure S18: Schematic representation for the synthesis procedure of FITC-tagged PAA-Cnp nanoparticles.

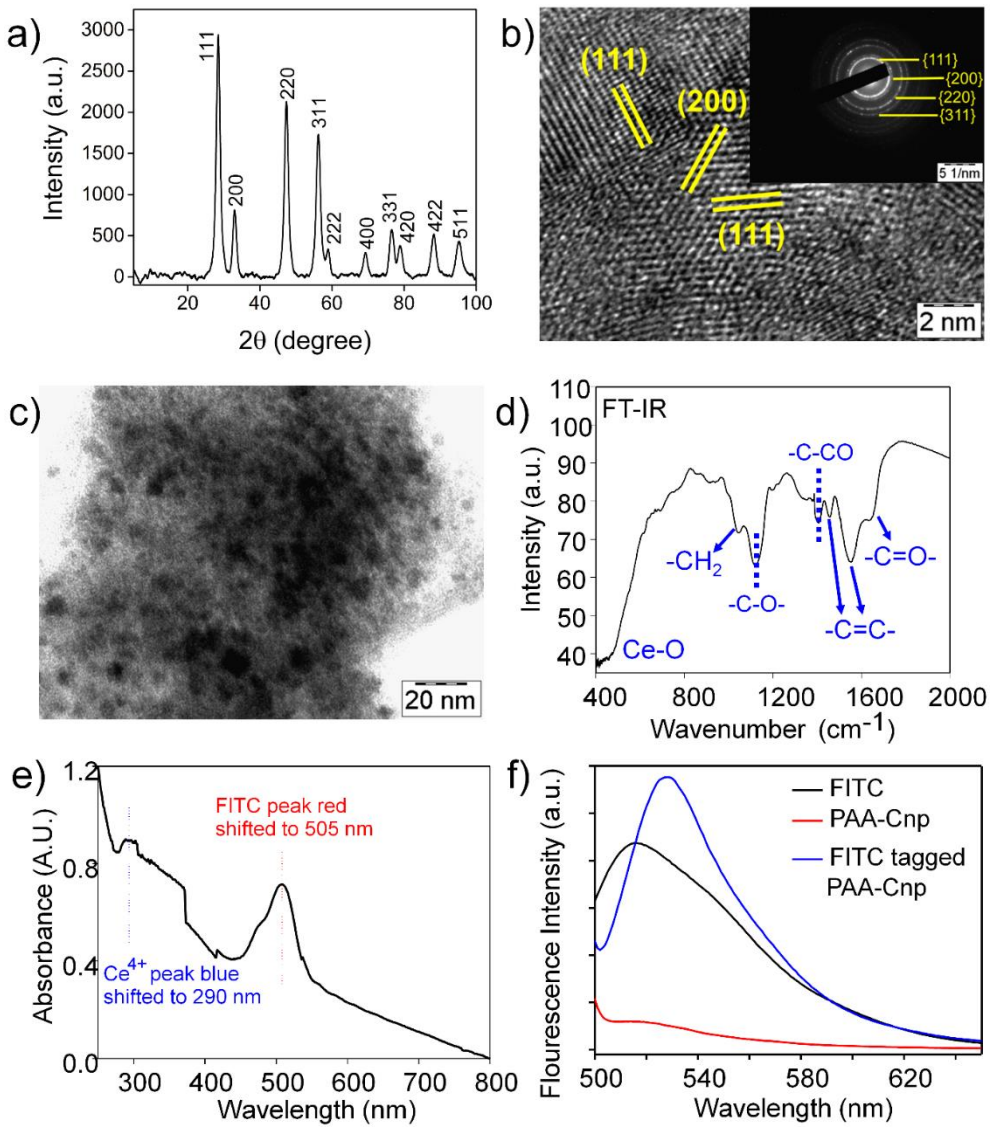

Figure S19: a) Powder XRD pattern of FITC-tagged PAA-Cnp showing cubic fluorite lattice. b-c) HRTEM and TEM images of FITC-tagged PAA-Cnp respectively. The HRTEM image and SAED pattern (inset) shows (111) and (200) planes. d) FT-IR spectrum of FITC-tagged PAA-Cnp shows presence of -C=C- indicating that PAA-Cnp was tagged with FITC. The characteristic peak for CeO_2 (Ce-O stretching) was observed at 460 cm^{-1} along with peaks for -C=O- and $-CH_2-$ stretching due to PAA. e) UV-Vis spectra of FITC-tagged PAA-Cnp shows absorbance maxima at 509 nm corresponding to FITC. f) Fluorescence emission spectra of FITC, PAA-Cnp and FITC-tagged PAA-Cnp showing emission maxima around 520 nm for FITC and FITC-tagged PAA-Cnp. Shift in the emission maxima observed for FITC-tagged PAA-Cnp compared to FITC is due to binding of FITC molecules on the surface of PAA-Cnp.

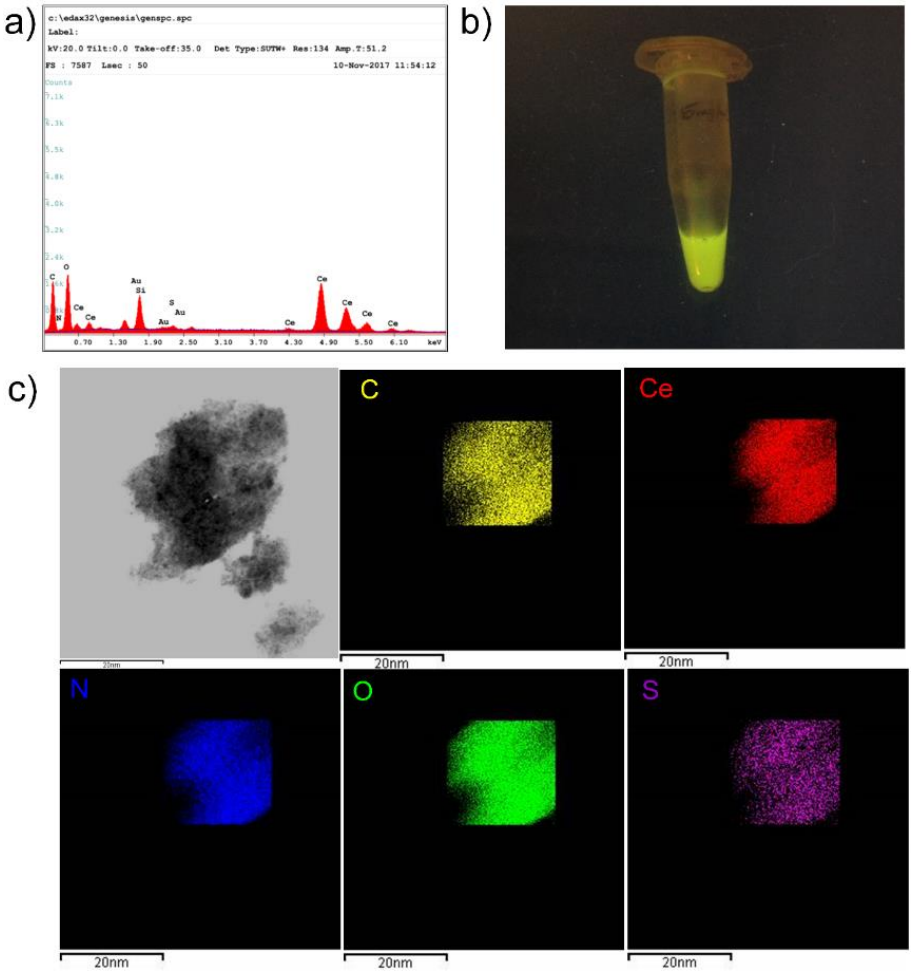

Figure S20: a) EDAX spectroscopic analysis of elemental composition of FITC-tagged PAA-Cnp. b) Photographic image of FITC-tagged PAA-Cnp dissolved in water showing fluorescence in blue UV-light. c) Elemental X-ray mapping of FITC-tagged PAA-Cnp showing distribution of elements C, Ce, N, O and S.

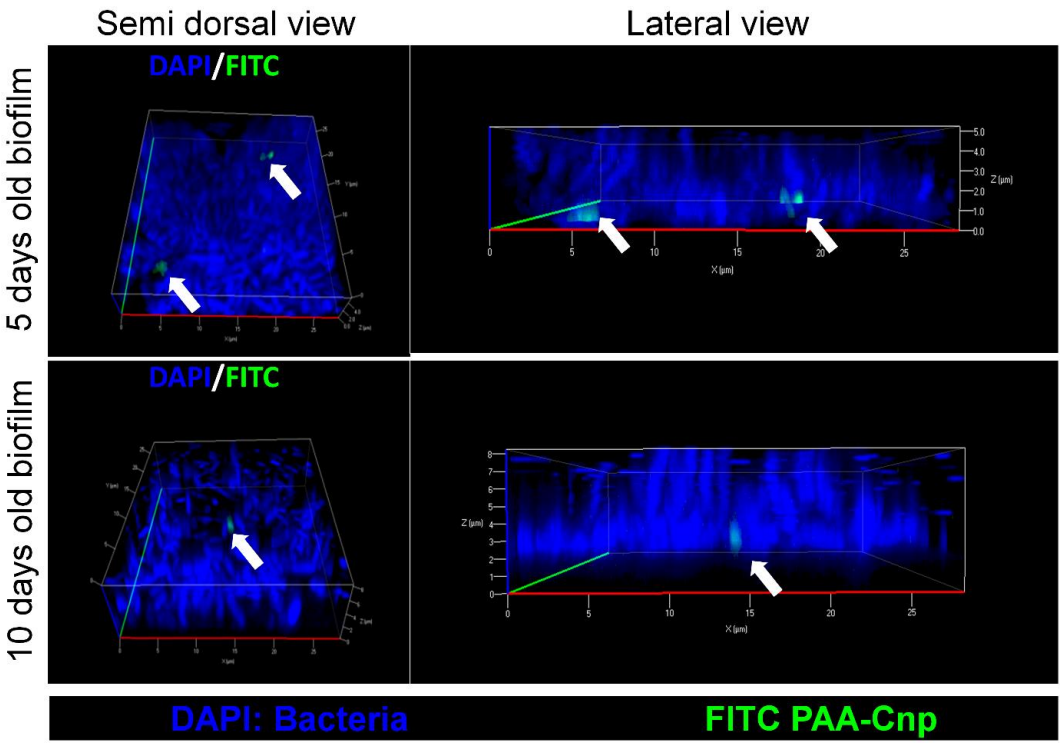

Figure S21: Representative 3D confocal images of pre-formed *Salmonella* biofilm grown till 5 days, or 10 days and post-treated with FITC-tagged PAA-Cnp. White arrows indicate the penetrated nanoparticles in the pre-formed biofilm.

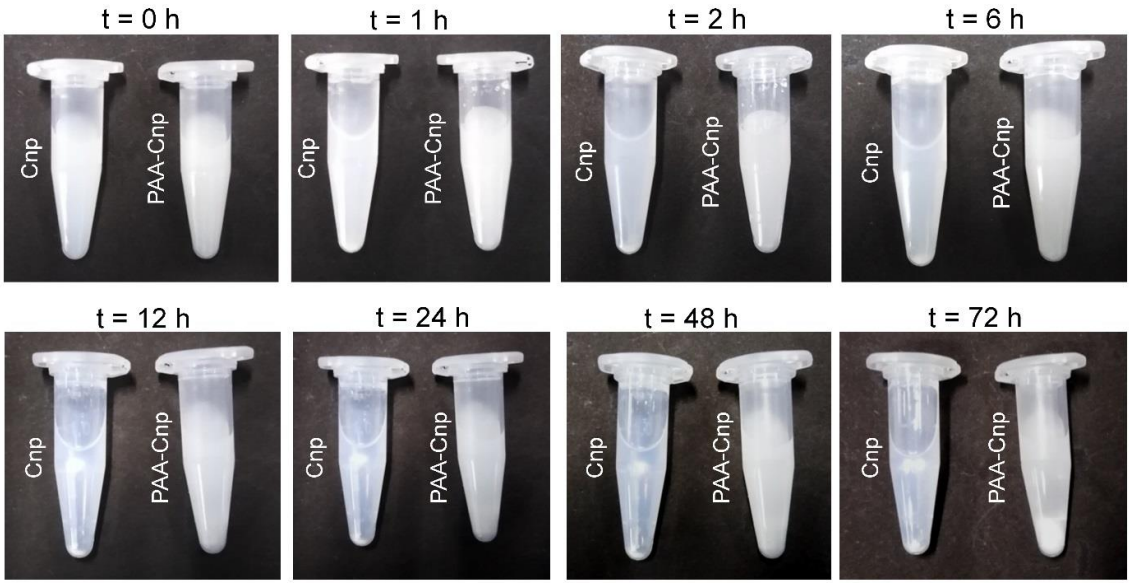

Figure S22: Dispersibility of Cnp and PAA Cnp in MQ water was monitored by time dependent imaging of the settling properties of the suspended nanoparticles.

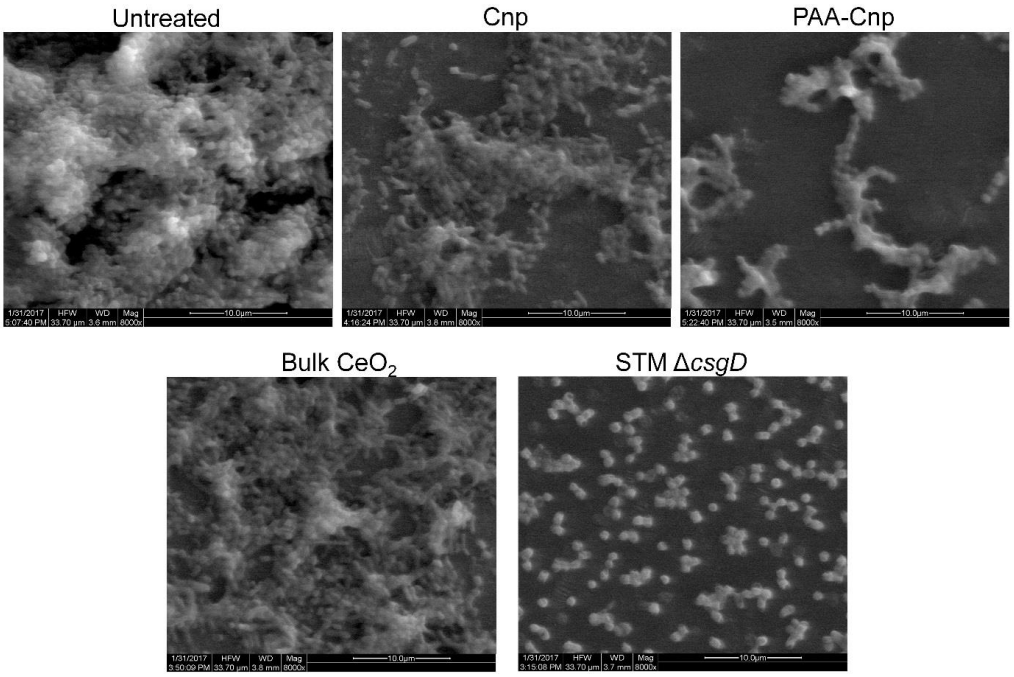

Figure S23: Scanning electron microscopy (SEM) images show *Salmonella* biofilm formed after 7 days with or without treatment of different forms of CeO_2. Scale bar=10 µm.

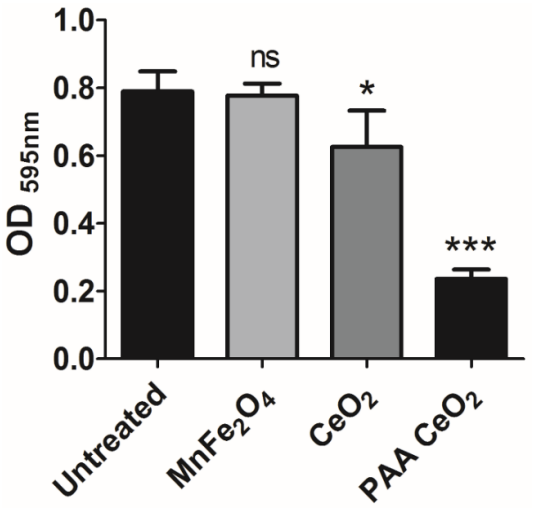

Figure S24: Bar diagram shows the quantification of biofilm formation based on crystal-violet staining assay among Cnp, PAA- Cnp and well-known oxidase mimetic, $MnFe_2O_4$ nanozyme. PAA-Cnp shows minimal biofilm formation compared to $MnFe_2O_4$ indicating that PAA-Cnp does not follow oxidase-like mechanism for the inhibition of biofilm formation. One way ANOVA with Bonferroni post test was used to analyse the results. P<0.001=***; P<0.01=**;P<0.05=* and P>0.05=ns.

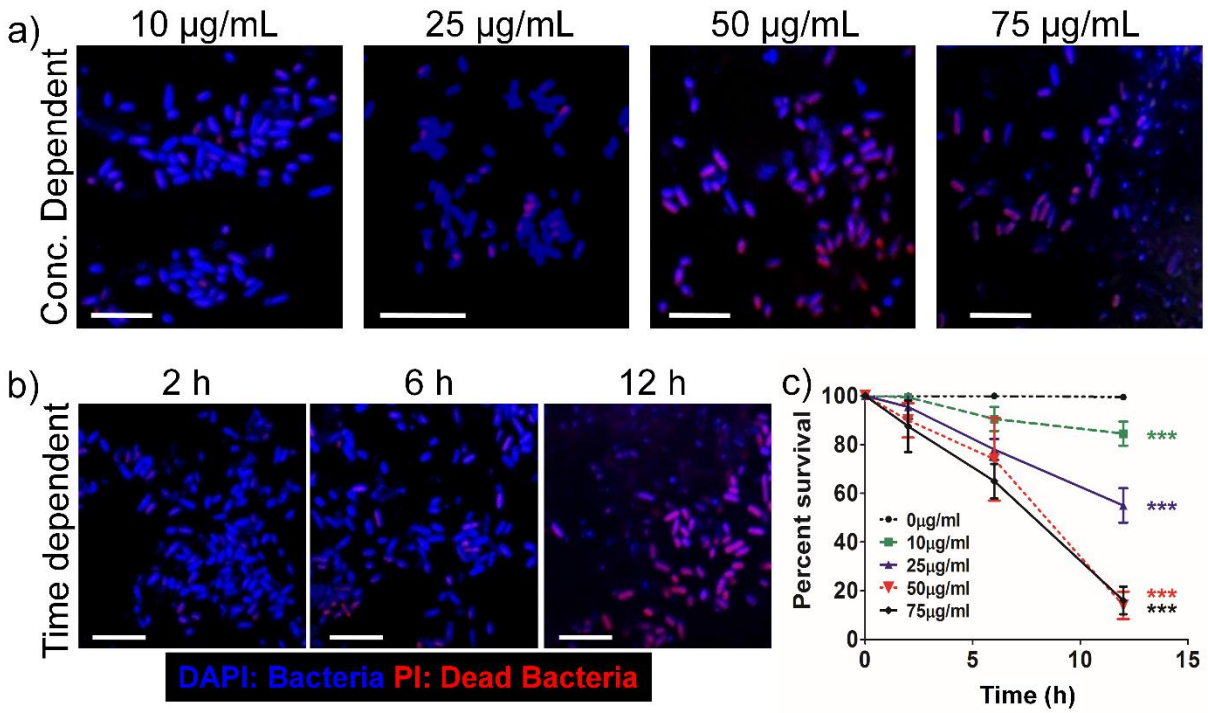

Figure S25: a) Representative confocal images of *E. Coli* treated with varying concentration of PAA-Cnp at the stationary phase. Images were acquired at fixed time point of 12 h after treatment. Greater antibacterial activity was observed with increasing concentration of the nanoparticle (≥ 50 µg/mL). b) Representative confocal images depicting the accumulation of dead cells over time treated with a fixed concentration of PAA-Cnp (50 µg/mL). Images were acquired at 2 h, 6 h, and 12 h from the treatment done at the stationary phase. c) Death curve representing % survival of bacteria as a function of time for varying dose of PAA-Cnp. The % survival was obtained by plating and enumerating CFU using, [(CFU t_n/CFU t_0)x100], where CFU t_n represent CFU at any given time after nanoparticle treatment and CFU t_0 represent CFU immediately after nanoparticle treatment. Treatment of nanoparticle was done at the stationary phase as described above. Less than 20% of surviving cells were observed after 12 h post-treatment from the stationary phase. Scale bar=10 µm.

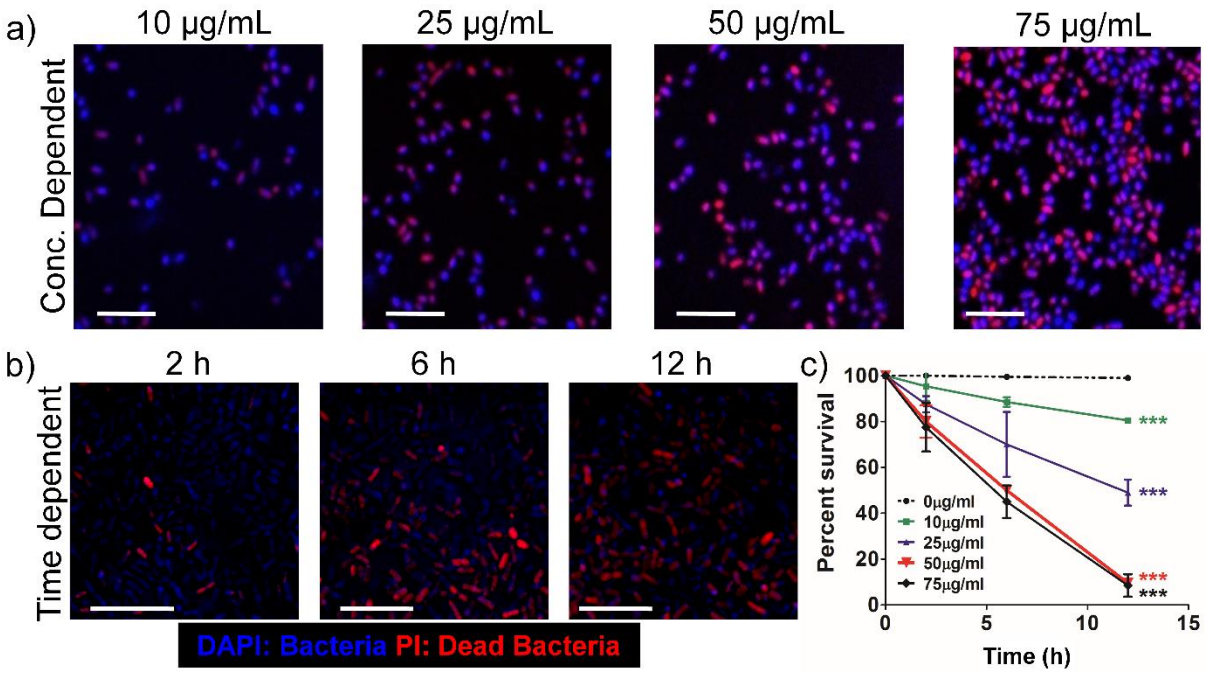

Figure S26: a) Representative confocal images of *Klebsiella pneumoniae* treated with varying concentration of PAA-Cnp at the stationary phase. Images were acquired at fixed time point of 12 h after treatment. Greater antibacterial activity was observed with increasing concentration of the nanoparticle (≥ 50 µg/mL). b) Representative confocal images depicting the accumulation of dead cells over time treated with a fixed concentration of PAA-Cnp (50 µg/mL). Images were acquired at 2 h, 6 h, and 12 h from the treatment done at the stationary phase. c) Death curve representing % survival of bacteria as a function of time for varying dose of PAA-Cnp. The % survival was obtained by plating and enumerating CFU using, [(CFU t_n/CFU t_0)x100], where CFU t_n represent CFU at any given time after nanoparticle treatment and CFU t_0 represent CFU immediately after nanoparticle treatment. Treatment of nanoparticle was done at the stationary phase as described above. Less than 10% of surviving cells were observed after 12 h post-treatment from the stationary phase. Scale bar=10 µm.

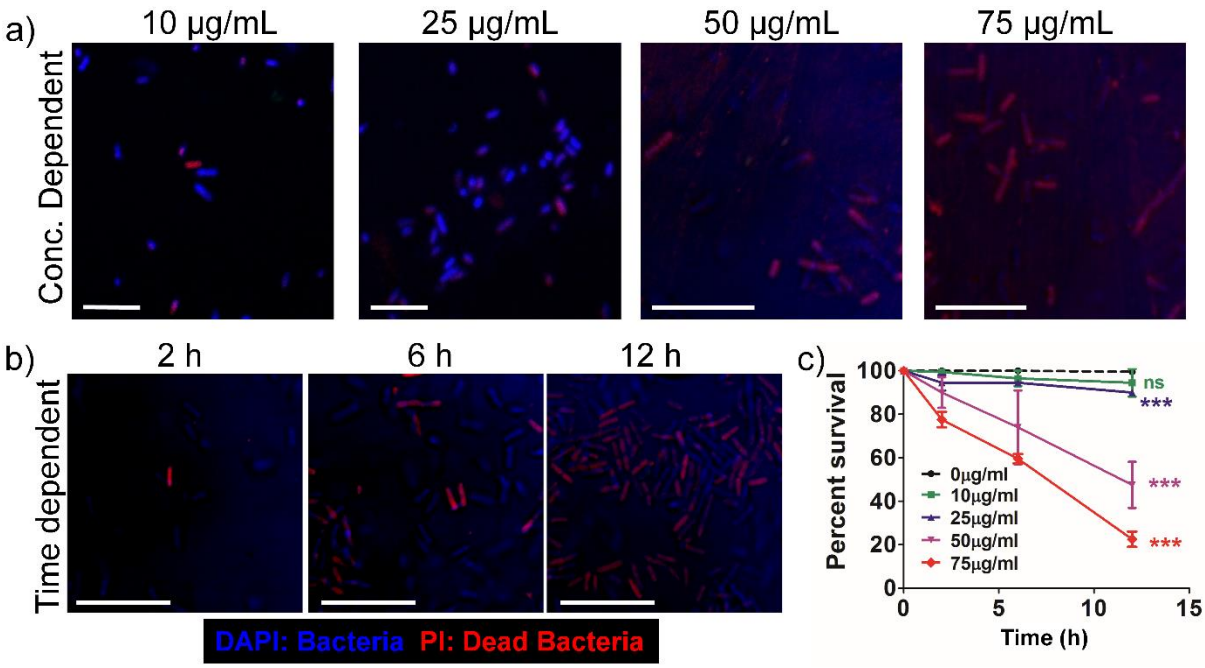

Figure S27: a) Representative confocal images of *Salmonella* Typhi treated with varying concentration of PAA-Cnp at the stationary phase. Images were acquired at fixed time point of 12 h after treatment. Greater antibacterial activity was observed at higher concentration of the nanoparticle (75 µg/mL). b) Representative confocal images depicting the accumulation of dead cells over time treated with a fixed concentration of PAA-Cnp (75 µg/mL). Images were acquired at 2 h, 6 h, and 12 h from the treatment done at the stationary phase. c) Death curve representing % survival of bacteria as a function of time for varying dose of PAA-Cnp. The % survival was obtained by plating and enumerating CFU using, [(CFU t_n/CFU t_0)x100], where CFU t_n represent CFU at any given time after nanoparticle treatment and CFU t_0 represent CFU immediately after nanoparticle treatment. Treatment of nanoparticle was done at the stationary phase as described above. Less than 20% of surviving cells were observed after 12 h post-treatment from the stationary phase. Scale bar=10 µm.

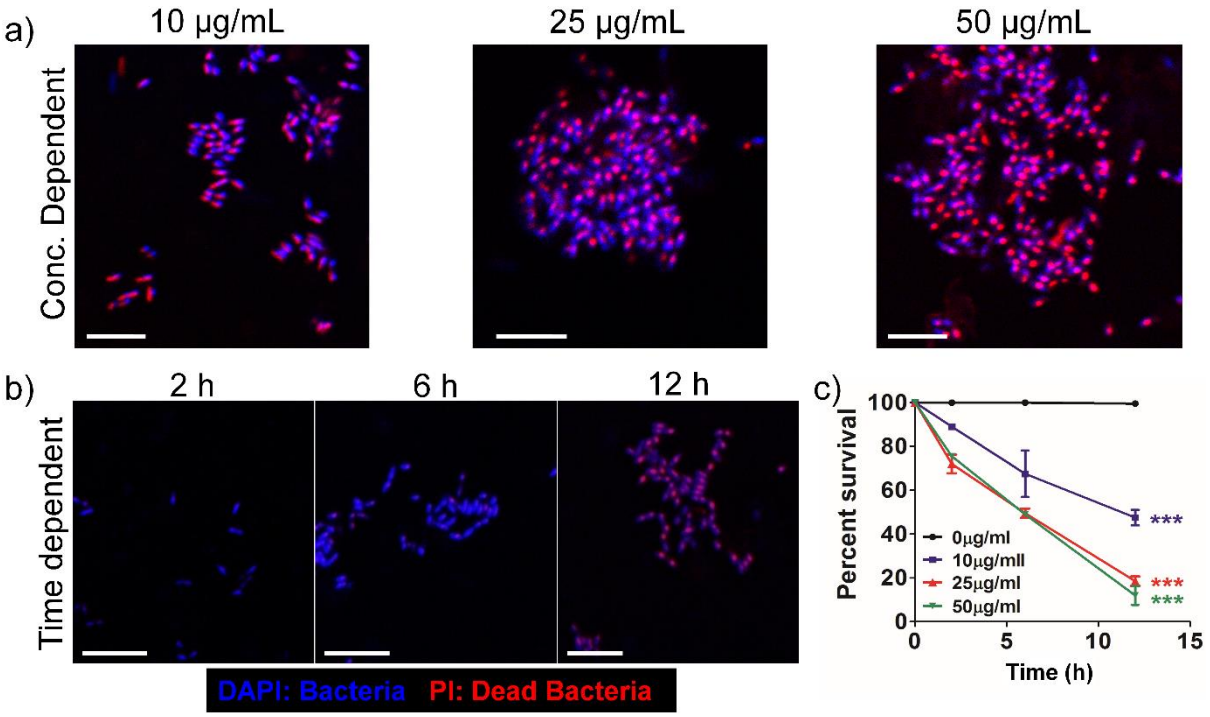

Figure S28: a) Representative confocal images of *Vibrio cholerae* treated with varying concentration of PAA-Cnp at the stationary phase. Images were acquired at fixed time point of 12 h after treatment. Greater antibacterial activity was observed with increasing concentration of the nanoparticle (≥ 25 µg/mL). b) Representative confocal images depicting the accumulation of dead cells over time treated with a fixed concentration of PAA-Cnp (25 µg/mL). Images were acquired at 2 h, 6 h, and 12 h from the treatment done at the stationary phase. c) Death curve representing % survival of bacteria as a function of time for varying dose of PAA-Cnp. The % survival was obtained by plating and enumerating CFU using, [(CFU t_n/CFU t_0)x100], where CFU t_n represent CFU at any given time after nanoparticle treatment and CFU t_0 represent CFU immediately after nanoparticle treatment. Treatment of nanoparticle was done at the stationary phase as described above. Less than 20% of surviving cells were observed after 12 h post-treatment from the stationary phase. Scale bar=10 µm.

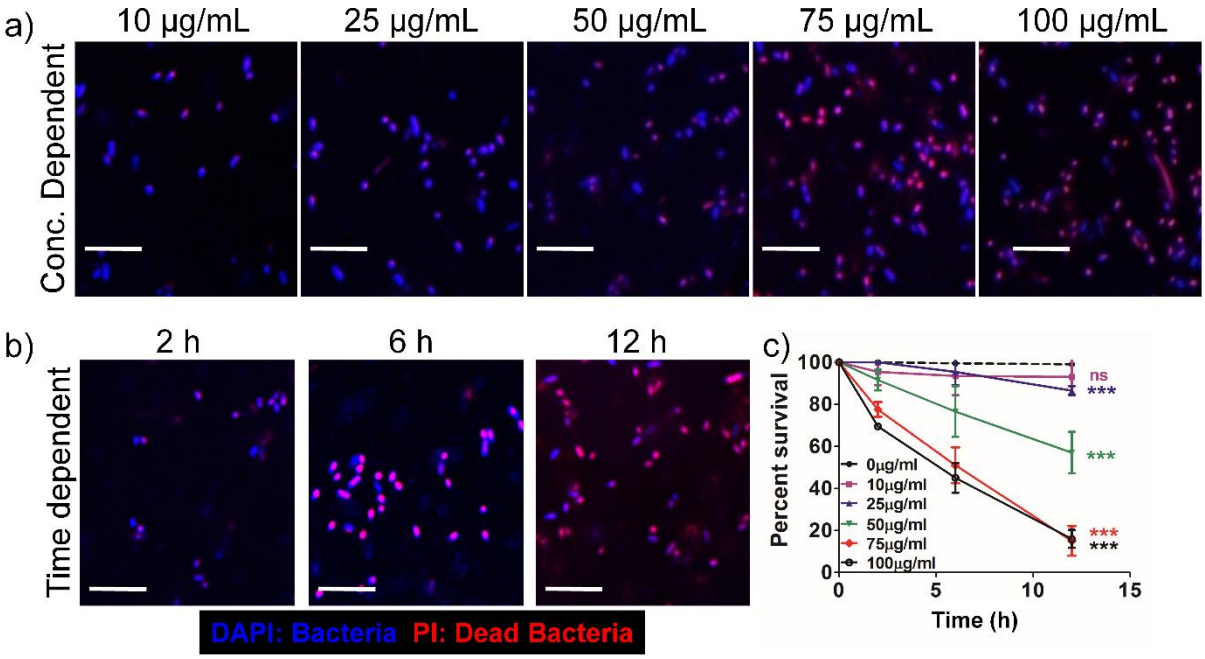

Figure S29: a) Representative confocal images of *Shigella flexneri* treated with varying concentration of PAA-Cnp at the stationary phase. Images were acquired at fixed time point of 12 h after treatment. Greater antibacterial activity was observed with increasing concentration of the nanoparticle (≥ 75 µg/mL). b) Representative confocal images depicting the accumulation of dead cells over time treated with a fixed concentration of PAA-Cnp (75 µg/mL). Images were acquired at 2 h, 6 h, and 12 h from the treatment done at the stationary phase. c) Death curve representing % survival of bacteria as a function of time for varying dose of PAA-Cnp. The % survival was obtained by plating and enumerating CFU using, [(CFU t_n/CFU t_0)x100], where CFU t_n represent CFU at any given time after nanoparticle treatment and CFU t_0 represent CFU immediately after nanoparticle treatment. Treatment of nanoparticle was done at the stationary phase as described above. Less than 20% of surviving cells were observed after 12 h post-treatment from the stationary phase. Scale bar=10 µm.

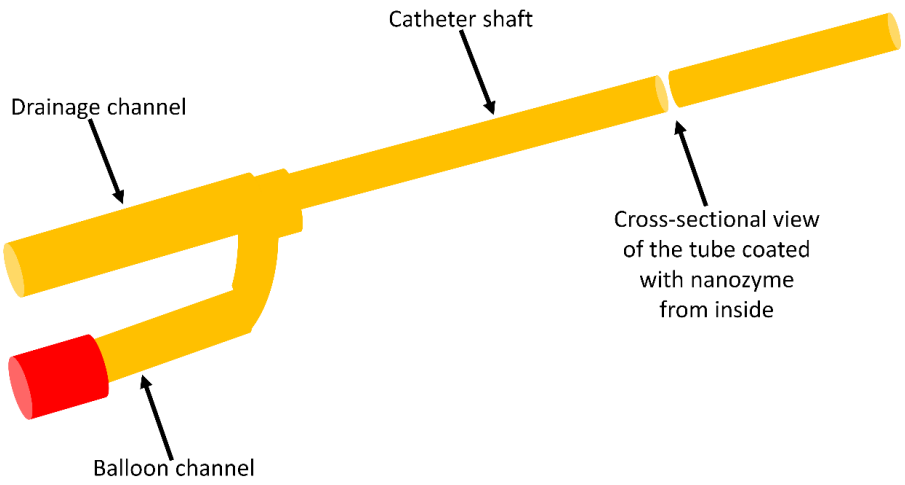

Figure S30: Representative image of the urinary catheter depicting the nanozyme coated region present in the interior of the catheter shaft.

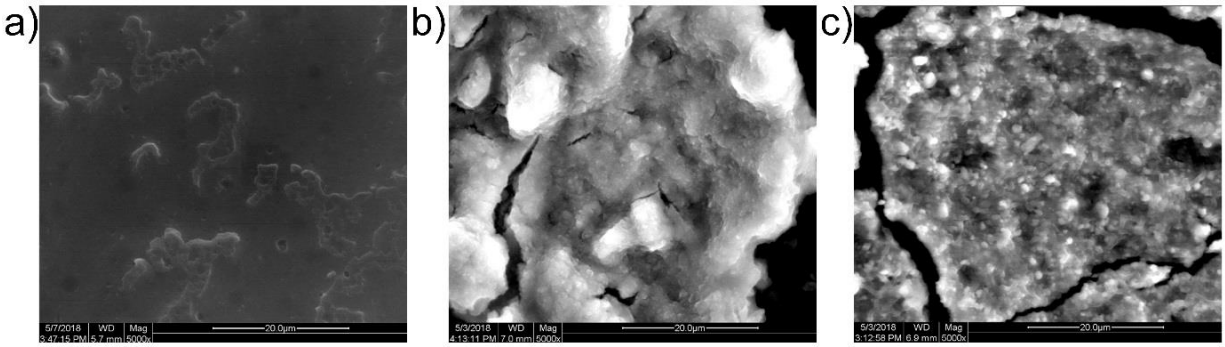

Figure S31: Scanning electron microscopy (SEM) images of catheters a) uncoated, b) coated with Cnp and c) coated with PAA-Cnp nanoparticles by means of drop-casting. SEM images of coated catheters prior incubation with the bacteria was used as control to visualize the condition of the catheters.

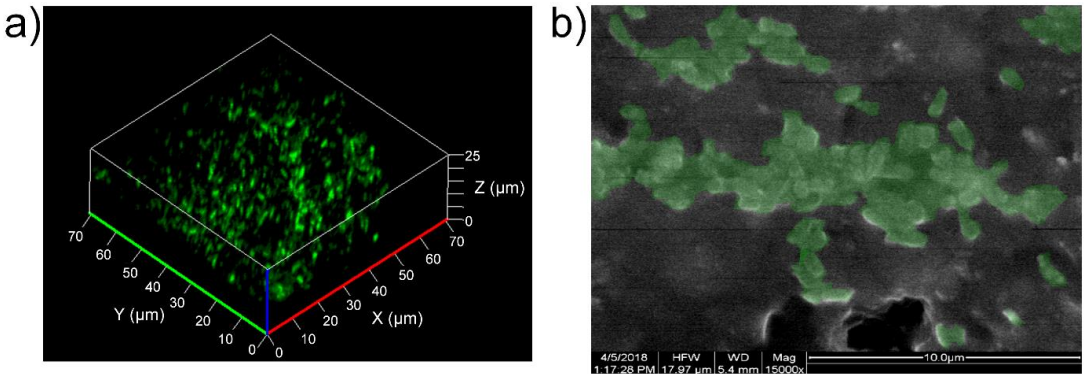

Figure S32: Representative a) confocal image and b) scanning electron microscopy (SEM) images respectively of biofilm formed by *Salmonella* on PAA-Cnp coated catheter.

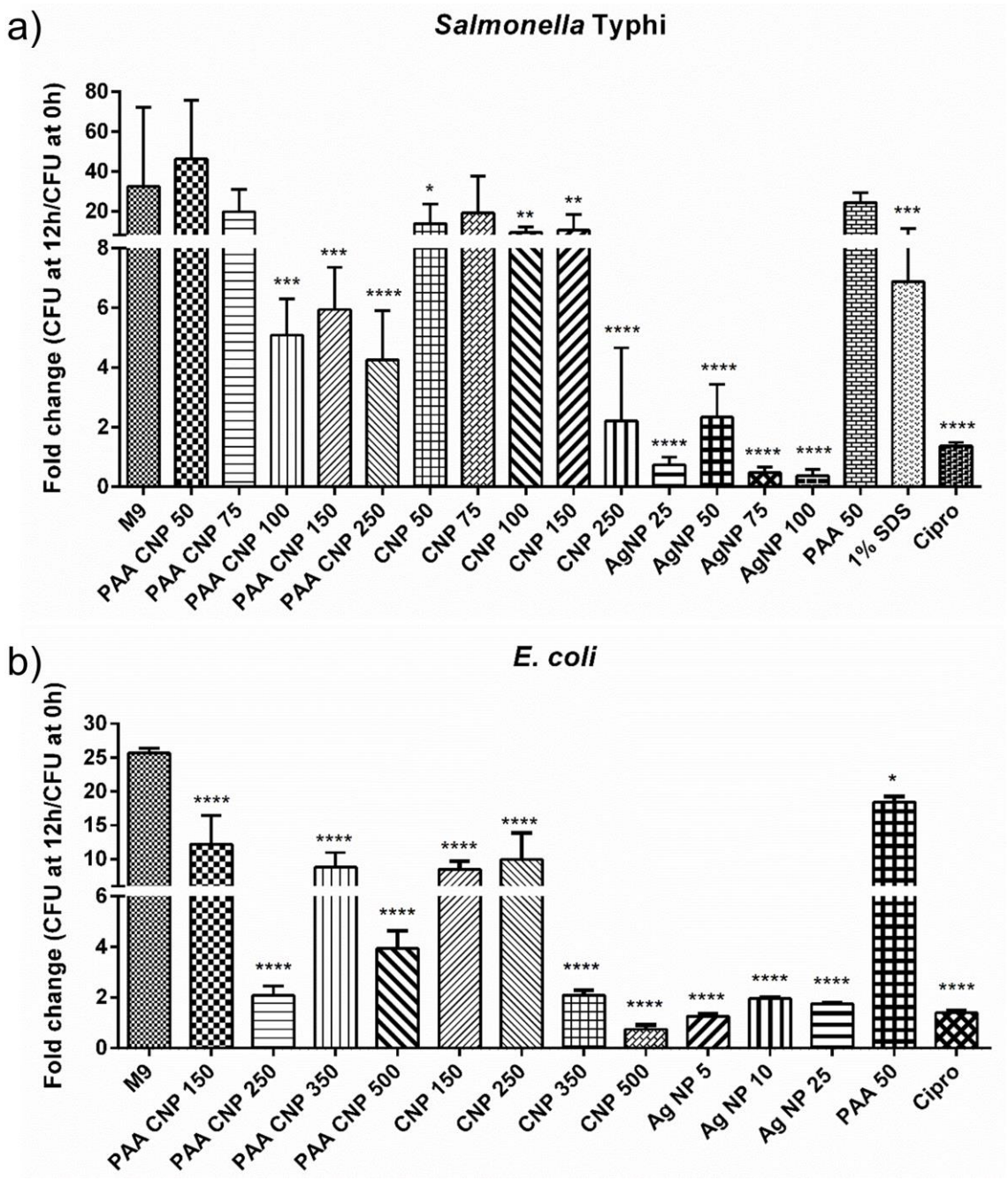

Figure S33: The antibacterial effect of the nanoparticles was checked by dilution plating technique for (a) *Salmonella Typhi* and (b) E. *coli*. The ratio of CFU at 12 h to 0 h was plotted for each nanoparticles. 5 µg/mL ciprofloxacin was used as positive control. Data are represented as mean + SEM of 3 independent experiments for case (a) and as mean + SEM of 2 independent experiments (b) One way ANOVA was used to analyse the data; p values ****<0.0001, ***<0.001, **<0.01, *<0.05.

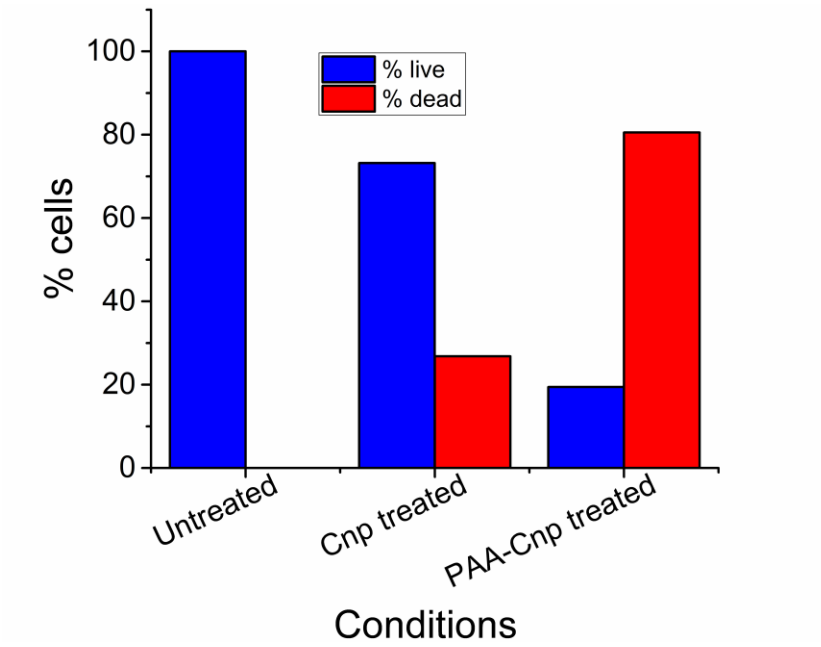

Figure S34: Quantification of % live and dead bacterial cells under different conditions based on PI staining assay given in figure 5b (main manuscript).

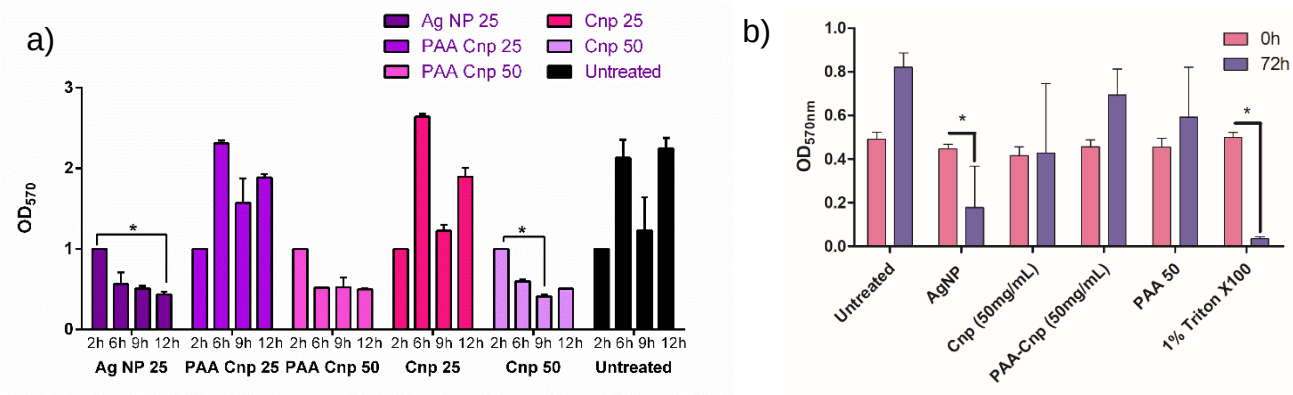

Figure S35: Cell viability assay using tetrazolium dye MTT. Cells were incubated for different time with the nanoparticles and checked for cell viability by measuring the absorbance of purple coloured formazan dye. Figure (a) and (b) represents early time point (2-12 hours) and late time point (72 hours) respectively. The increase in the OD in some of the wells, could be resulted from proliferation of the immortalized HeLa cells. Two way ANOVA was used to analyse the data; p values *<0.05.